



1 **Impact of HO₂ aerosol uptake on radical levels and O₃** 2 **production during summertime in Beijing**

3 Joanna E. Dyson¹, Lisa K. Whalley^{1,2*}, Eloise J. Slater^{1,a}, Robert Woodward-Masse¹,
4 Chunxiang Ye³, James D. Lee^{4,5}, Freya Squires^{4,b}, James R. Hopkins^{4,5}, Rachel E. Dunmore⁴,
5 Marvin Shaw^{4,5}, Jacqueline F. Hamilton⁴, Alastair C. Lewis^{4,5}, Stephen D. Worrall⁶, Asan
6 Bacak⁷, Archit Mehra^{8,c}, Thomas J. Bannan⁸, Hugh Coe^{8,9}, Carl J. Percival¹⁰, Bin Ouyang¹¹, C.
7 Nicholas Hewitt¹¹, Roderic L. Jones¹², Leigh R. Crilley¹³, Louisa J. Kramer¹⁴, W. Joe. F.
8 Acton¹⁴, William J. Bloss¹⁴, Supattarachai Saksakulkrai¹⁴, Jingsha Xu^{14,d}, Zongbo Shi¹⁴, Roy
9 M. Harrison^{14,e}, Simone Kotthaus^{15,16}, Sue Grimmond¹⁵, Yele Sun¹⁷, Weiqi Xu¹⁷, Siyao
10 Yue^{17,18,19}, Lianfang Wei^{17,19}, Pingqing Fu^{17,18}, Xinming Wang²⁰, Stephen R. Arnold²¹,
11 Dwayne E. Heard^{1*}

12 *[1] School of Chemistry, University of Leeds, LS2 9JT, UK.*

13 *[2] National Centre of Atmospheric Science, University of Leeds, LS2 9JT, UK.*

14 *[3] College of Environmental Sciences and Engineering, Peking University, Beijing, 100871,*
15 *China.*

16 *[4] Wolfson Atmospheric Chemistry Laboratories, Department of Chemistry, University of*
17 *York, Heslington, York, YO10 5DD, UK.*

18 *[5] National Centre of Atmospheric Science, University of York, Heslington, York, YO19 5DD,*
19 *UK.*

20 *[6] Aston Institute of Materials Research, School of Engineering and Applied Science, Aston*
21 *University, Birmingham, B4 7ET, UK.*

22 *[7] Turkish Accelerator and Radiation Laboratory, Ankara University Institute of Accelerator*
23 *Technologies, Atmospheric and Environmental Chemistry Laboratory, Gölbaşı Campus,*
24 *Ankara, Turkey.*

25 *[8] Centre of Atmospheric Sciences, School of Earth and Environmental Sciences, University*
26 *of Manchester, Manchester, M13 9PL, UK.*

27 *[9] National Centre for Atmospheric Sciences, University of Manchester, Manchester, M13*
28 *9PL, UK.*



- 29 [10] Jet Propulsion Laboratory, California Institute of Technology, Pasadena, CA, USA.
- 30 [11] Lancaster Environment Centre, Lancaster University, Lancaster, LA1 4YW, UK.
- 31 [12] Department of Chemistry, University of Cambridge, Cambridge, UK.
- 32 [13] Department of Chemistry, York University, Toronto, ON, M3J 1P3, Canada.
- 33 [14] School of Geography, Earth and Environmental Sciences, University of Birmingham,
34 Birmingham, B15 2TT, UK.
- 35 [15] Department of Meteorology, University of Reading, Reading, UK.
- 36 [16] Institut Pierre Simon Laplace, École Polytechnique, Palaiseau, France.
- 37 [17] State Key Laboratory of Atmospheric Boundary Layer Physics and Atmospheric
38 Chemistry, Institute for Atmospheric Physics, Chinese Academy of Sciences, Beijing 100029,
39 China.
- 40 [18] Institute of Surface-Earth System Science, School of Earth System Science, Tianjin
41 University, Tianjin 300072, China.
- 42 [19] Minerva Research Group, Max Planck Institute for Chemistry, 55128 Mainz, Germany.
- 43 [20] State Key Laboratory of Organic Geochemistry, Guangzhou Institute of Geochemistry,
44 Chinese Academy of Sciences, Guangzhou, 510640, China.
- 45 [21] School of Earth and Environment, University of Leeds, LS2 9JT, UK.
- 46 ^anow at: The Hut Group, Unit 1 Icon Manchester, Manchester Airport, WA15 0AF, UK.
- 47 ^bnow at: British Antarctic Survey, Cambridge, CB3 0ET, UK.
- 48 ^cnow at: Chaucer, Part of Bip Group, 10 Lower Thames Street, London, EC3R 6EN^dnow at:
49 Beijing Hanzhou Innovation Institute Yuhang, Xixi Octagon City, Yuhang District, Hangzhou
50 310023, China.
- 51 ^ealso at: Department of Environmental Sciences, Faculty of Meteorology, Environment and
52 Arid Land Agriculture, King Abdulaziz University, Jeddah, Saudi Arabia.
- 53 *Correspondence to: D.E.Heard@leeds.ac.uk, L.K.Whalley@leeds.ac.uk

54

55



56 **Abstract** The impact of heterogeneous uptake of HO₂ onto aerosol surfaces on radical
57 concentrations and the O₃ production regime in Beijing summertime was investigated. The
58 uptake coefficient of HO₂ onto aerosol surfaces, γ_{HO_2} , was calculated for the AIRPRO
59 campaign in Beijing, Summer 2017, as a function of measured aerosol soluble copper
60 concentration, [Cu²⁺]_{eff}, aerosol liquid water content, [ALWC], and particulate matter
61 concentration, [PM]. An average γ_{HO_2} across the entire campaign of 0.070 ± 0.035 was
62 calculated, with values ranging from 0.002 to 0.15, and found to be significantly lower than
63 the value of $\gamma_{HO_2} = 0.2$, commonly used in modelling studies. Using the calculated γ_{HO_2} values
64 for the Summer AIRPRO campaign, OH, HO₂ and RO₂ radical concentrations were modelled
65 using a box-model incorporating the Master Chemical Mechanism (v3.3.1), with and without
66 the addition of γ_{HO_2} , and compared to the measured radical concentrations. Rate of destruction
67 analysis showed the dominant HO₂ loss pathway to be HO₂ + NO for all NO concentrations
68 across the Summer Beijing campaign with HO₂ uptake contributing < 0.3 % to the total loss of
69 HO₂ on average. This result for Beijing summertime would suggest that under most conditions
70 encountered, HO₂ uptake onto aerosol surfaces is not important to consider when investigating
71 increasing O₃ production with decreasing [PM] across the North China Plain. At low [NO],
72 however, i.e. < 0.1 ppb, which was often encountered in the afternoons, up to 29% of modelled
73 HO₂ loss was due to HO₂ uptake on aerosols when calculated γ_{HO_2} was included, even with the
74 much lower γ_{HO_2} values compared to $\gamma_{HO_2} = 0.2$, a results which agrees with the aerosol-
75 inhibited O₃ regime recently proposed by Ivatt et al., 2022. As such it can be concluded that in
76 cleaner environments, away from polluted urban centres where HO₂ loss chemistry is not
77 dominated by NO but where aerosol surface area is high still, changes in PM concentration and
78 hence aerosol surface area could still have a significant effect on both overall HO₂
79 concentration and the O₃ production regime.

80 Using modelled radical concentrations, the absolute O₃ sensitivity to NO_x and VOC showed
81 that, on average across the summer AIRPRO campaign, the O₃ production regime remained
82 VOC-limited, with the exception of a few days in the afternoon when the NO mixing ratio
83 dropped low enough for the O₃ regime to shift towards NO_x-limited. The O₃ sensitivity to VOC,
84 the dominant regime during the summer AIRPRO campaign, was observed to decrease and
85 shift towards a NO_x sensitive regime both when NO mixing ratio decreased and with the
86 addition of aerosol uptake. This suggests that if [NO_x] continues to decrease in the future, ozone
87 reduction policies focussing solely on NO_x reductions may not be as efficient as expected if



88 [PM] and, hence, HO₂ uptake to aerosol surfaces, continues to decrease. The addition of aerosol
89 uptake into the model, for both the γ_{HO_2} calculated from measured data and when using a fixed
90 value of $\gamma_{HO_2} = 0.2$, did not have a significant effect on the overall O₃ production regime across
91 the campaign. While not important for this campaign, aerosol uptake could be important for
92 areas of lower NO concentration that are already in a NO_x-sensitive regime.

93 **1 Introduction**

94 Climate change and air quality are two significant environmental issues faced by society today
95 with the drive to net zero emissions by 2050 becoming increasingly important to remain
96 consistent with the long-term anthropogenic temperature warming outcome of below 1.5 °C as
97 set out by the Paris Agreement in 2016. Increasing anthropogenic emissions have caused not
98 only an increase in atmospheric warming, but also a deterioration in atmospheric air quality: a
99 concern due to both short and long term negative health effects seen as a product of poor air
100 quality such as respiratory and cardiovascular diseases and cancer (Brauer et al., 2016; Gakidou
101 et al., 2017), in addition to a variety of negative effects on the environment such as increased
102 soil acidification and the ensuing damage to vegetation and crop yield as a by-product of
103 increasing acidity of rain (Forster et al., 2007).

104 Ambient air pollution has become a serious issue globally, specifically in large urban areas
105 effected by anthropogenic emission sources. Due to rapid industrialisation, Chinese megacities
106 in particular face significant environmental and health challenges from the decline in air quality
107 following urbanisation, with areas such as the Beijing-Tianjin-Hebei area in the North China
108 Plain (NCP) suffering from seasonal extreme pollution episodes as a consequence (Wang,
109 2021; Jin et al., 2016). In terms of human health, the most important pollutants in many regions
110 are ground level O₃, NO_x (NO₂ and NO) and particulate matter. Nitrogen dioxide (NO₂) can be
111 directly emitted into the atmosphere from high temperature combustion sources or can be
112 formed via the reaction of nitrogen monoxide (NO) with an oxidising species in the
113 troposphere, such as HO₂, leading to the formation of hydroxyl radical (OH) (Ye et al., 2017).
114 Ozone, while vital in the stratosphere to protect the earth from harmful UV radiation and
115 excessive planetary heating, is toxic to both plant and human life at ground level and can react
116 with NO to form NO₂. Particulate matter is emitted anthropogenically and biogenically and can
117 play a role in the warming and cooling of the atmosphere due to the ability of aerosols to absorb
118 or scatter IR radiation depending on their composition. High levels of particulate matter, NO_x



119 and tropospheric O₃ in areas of low atmospheric mixing lead to photochemical smog and the
120 reduction of visibility characteristic of extreme pollution episodes.

121 The concentration of pollutants and trace gases in the troposphere is controlled not only by
122 emission levels but also by the oxidation capacity of the atmosphere which is determined
123 largely by the concentration of the hydroxyl radical (OH) and the closely coupled hydroperoxyl
124 (HO₂) radical, referred to collectively as HO_x radicals. Known for their role in chemical
125 oxidation processes in the atmosphere, OH and HO₂ are vital species when considering climate
126 change and air pollution. The OH radical is the main daytime tropospheric oxidant, with a
127 major role as a source of ground level ozone (O₃) (Levy, 1971) and as a sink for both
128 atmospheric pollutants, such as methane, and other radical species. The OH radical also has a
129 role in the formation of secondary pollutants including secondary organic aerosols (SOAs)
130 formed via the oxidation of volatile organic compounds (VOCs). OH and HO₂ radicals are
131 closely linked, due to the recycling of HO₂ to give OH, either via the reaction with NO or CO,
132 with the dominant loss pathway of HO₂ in polluted regions being the reaction with NO to form
133 OH (for example, as shown in Beijing by Slater et al., 2020; Whalley et al., 2021). As such,
134 understanding the sources and sinks of both OH and HO₂ within the troposphere is crucial to
135 fully understand the concentration and distribution of trace atmospheric species associated with
136 climate change and poor air quality.

137 Observed HO₂ concentrations from field measurements frequently can-not be fully explained
138 by atmospheric chemistry models which often have a tendency to over-predict HO₂ in low NO_x
139 conditions (Kanaya et al., 2007; Commane et al., 2010; Whalley et al., 2010; Whalley et al.,
140 2021; Slater et al., 2020; Sommariva et al., 2004). Following the ClearfLo campaign in London
141 2012, zero-dimensional modelling showed an over-prediction of HO₂ by up to a factor of 10 at
142 low NO_x which was attributed to uncertainties in the degradation mechanism of complex
143 biogenic and diesel-related VOC species at low NO_x (Whalley et al., 2018). Over-prediction of
144 HO₂ is also commonly thought to be due, in part, to lack of understanding of HO₂ uptake onto
145 aerosol surfaces. A 2014 modelling study by Xue et al., 2014 focussing on the transport,
146 heterogeneous chemistry and precursors of ground level ozone in Beijing, Shanghai,
147 Guangzhou and Lanzhou, identified HO₂ uptake as a source of uncertainty when considering
148 ozone production, with uptake onto aerosols having the largest effect on HO₂ concentration in
149 Beijing where aerosol loadings were the highest.



150 While the impact of HO₂ uptake on HO_x concentrations has been calculated to vary from ~10-
151 40 % (Jacob, 2000; Whalley et al., 2010; Whalley et al., 2021; Slater et al., 2020; Mao et al.,
152 2010; Li et al., 2019; Li et al., 2018) globally, often a single value of $\gamma_{HO_2} = 0.2$ is used within
153 models, as recommended by Jacob, 2000. Previous experimental studies report uptake
154 coefficients which span several orders of magnitude, however, and vary largely based on the
155 state of the aerosol and whether transition metal ion catalysis is involved. For dry inorganic
156 salt aerosols values as low as $\gamma_{HO_2} < 0.002$ have been reported (Cooper and Abbatt, 1996;
157 Taketani et al., 2008; George et al., 2013) increasing to up to $\gamma_{HO_2} = 0.2$ for aqueous aerosols
158 (Thornton and Abbatt, 2005; Taketani et al., 2008; George et al., 2013). Previous experimental
159 studies report much higher $\gamma_{HO_2} > 0.4$ for Cu-doped aqueous aerosols (Thornton and Abbatt,
160 2005; Mozurkewich et al., 1987; Taketani et al., 2008; George et al., 2013; Lakey et al., 2016).
161 Recently, larger values of γ_{HO_2} have been measured experimentally from samples taken offline
162 at Mt. Tai (0.13-0.34) and Mt. Mang (0.09-0.40) in China by Taketani et al., 2012, while
163 another study in Kyoto, Japan, directly measured γ_{HO_2} values under ambient conditions from
164 0.08 to 0.36 (Zhou et al., 2020). With $\gamma_{HO_2} > 0.1$, HO₂ concentrations can be significantly
165 influenced particularly in areas of low [NO] and/or high aerosol loadings (Lakey et al., 2015;
166 Matthews et al., 2014; Mao et al., 2013; Zhou et al., 2021; Martinez et al., 2003).

167 Following multiple policies implemented across China in response to the poor air quality
168 “crisis”, a number of studies have reported a decrease in NO_x and PM_{2.5} emissions in China
169 (Jin et al., 2016). Liu et al., 2017 reported NO_x (NO₂ + NO) emissions over 48 Chinese cities
170 to have decreased by 21 % in the period of 2011-2015, supported by observed declines in NO_x
171 emissions reported by other studies (Krotkov et al., 2016; Liu et al., 2016; Miyazaki et al.,
172 2017; Van Der A et al., 2017). Ma et al., 2016b reported a mean annual decrease in PM_{2.5} of
173 0.46 $\mu\text{g m}^{-3}$ between 2008-2013, while Lin et al., 2018 reported an average decrease of 0.65
174 $\mu\text{g m}^{-3} \text{ yr}^{-1}$ between 2006-2010 increasing to a decline of 2.33 $\mu\text{g m}^{-3} \text{ yr}^{-1}$ for the period of
175 2011-2015. In contrast to the observed decrease in NO_x and PM_{2.5} emissions, several studies
176 have reported increasing O₃ levels. Ma et al., 2016a reported a maximum daily average 8h
177 mean (MDA8) increase in O₃ concentrations of 1.13 ppb yr^{-1} for the period between 2003-2015
178 at a rural site north of Beijing while satellite observations suggested ground level ozone had
179 increased ~7% for the period between 2005-2010 (Verstraeten et al., 2015). A recent study by
180 Silver et al., 2018 also observed a significant increase in O₃ concentrations with median MDA8
181 increasing at a rate of 4.6 $\mu\text{g m}^{-3} \text{ yr}^{-1}$ across China.



182 A 2018 modelling study using the regional model GEOS-Chem by Li et al., 2018 suggested
183 the increase in O₃ across China between 2013-2017 could be attributed to the decrease in PM_{2.5},
184 with changes in PM_{2.5} being a more important driver of increasing O₃ trends than NO_x and
185 VOC emissions for the period studied. It was proposed that a decrease in PM_{2.5} emissions had
186 led to a decrease in loss of HO₂ via aerosol uptake resulting in an increase in HO₂ concentration,
187 and a proportional increase in the loss of HO₂ via NO leading to NO₂ which, when photolyzed,
188 forms O₃ leading to an increase in O₃ (Li et al., 2018). However, analysis of measured radical
189 budget from a field campaign in the North China Plain in Summer 2014 with a calculated γ_{HO_2}
190 of 0.08 ± 0.13 , showed no evidence for a significant impact of HO₂ heterogeneous chemistry
191 on radical concentrations in North China Plain, concluding that reduced HO₂ uptake was
192 unlikely to therefore be the cause of increasing O₃ levels in the North China Plain (Tan et al.,
193 2020). Using a novel parameterisation developed by Song et al., 2020 in the framework of the
194 resistor model to take into account the influence of aerosol soluble copper, aerosol liquid water
195 content and particulate matter concentration on HO₂ uptake, and the Multiphase Chemical
196 Kinetic box model (PKU-MARK) to assess the impact of HO₂ uptake on the O₃ budget for
197 Wangdu Campaign in 2014, Song et al., 2022 concluded that HO₂ heterogeneous processes
198 could decrease the O₃ production rates by up to 6 ppbv hr⁻¹, particularly in the morning VOC-
199 limited regime.

200 In this study, the new parameterisation introduced by Song et al., 2021, hereafter referred to
201 solely as the Song parameterisation, coupled with measured data from the Summer AIRPRO
202 campaign in Beijing 2017 was used to calculate a time series of the HO₂ uptake coefficient,
203 which was then used to investigate the impact of heterogeneous uptake of HO₂ onto aerosol
204 surfaces on the HO₂ radical budget in Summertime Beijing using the Master Chemical
205 Mechanism and the impact on the O₃ regime. We will test the hypothesis that reduced HO₂
206 uptake due to a reduction in PM_{2.5} concentration is a significant driver of the recent increase in
207 ozone concentrations in China.

208 **2 Experimental**

209 **2.1 Campaign overview and site description**

210 As part of the Atmospheric Pollution and Human Health (APHH) in a Chinese Megacity
211 programme, the University of Leeds took simultaneous measurements of OH, HO₂, RO₂ and
212 OH reactivity (k_{OH}), in addition to measurements of HCHO and photolysis rates, during two



213 field campaigns at an urban site in Winter 2016 and Summer 2017 in Beijing, with the aim to
214 study the chemical and physical processes governing gas and particle pollution and
215 meteorological dynamics in the Beijing region and the links between the two (Shi et al., 2019;
216 Slater et al., 2020; Whalley et al., 2021). The two field campaigns in Beijing were part of the
217 AIRPRO (The integrated study of AIR pollution PROCesses in Beijing) project within the
218 APHH programme, described fully by Shi et al., 2019.

219 For the summer AIRPRO campaign, the official science period was from 23rd May 2017 to the
220 22nd June 2017, with observations taking place at the Institute of Atmospheric Physics (IAP)
221 within the Chinese Academy of Sciences, located between the third and fourth ring roads in
222 central Beijing within 100 m of a major road, making local traffic emission sources an
223 important source of pollution during measurement period. All instrumentation for the campaign
224 was located at this site, housed within nine shipping containers surrounding a meteorological
225 tower. Further details of the instrumentation and measurement site can be found in Shi et al.,
226 2019.

227 **2.2 FAGE instrumentation description**

228 The University of Leeds Fluorescence Assay by Gas Expansion (FAGE) instrument made
229 measurements of OH, HO₂ and RO₂ radicals and OH reactivity (*k_{OH}*). The FAGE instrument
230 set up is described fully in Whalley et al., 2018 while the OH reactivity instrument set up is
231 described fully in Whalley et al., 2016. Both instruments are also described fully in Slater et
232 al., 2020 and so only a brief description is given here.

233 Two cells, a HO_x cell and a RO_x cell connected together with a side arm, were used to take
234 radical measurements from the roof of the Leeds FAGE lab container. A RO_xLIF flow reactor
235 was also coupled to the RO_x cell to allow for detection of RO₂ (total, complex and simple) as
236 described by Fuchs et al., 2008. The HO_x cell took sequential measurements of OH and the
237 sum of OH and HO₂, by the addition of NO (Messer, 99.5 %), which titrated HO₂ to OH for
238 detection by Laser Induced Fluorescence (LIF) at 308 nm.

239 The RO_xLIF reactor operated in 2 modes: a ‘HO_x mode’ where a flow of CO (10 % in N₂) was
240 added to ambient sampled air close to the pin hole to convert all ambient OH to HO₂; and a
241 ‘RO_x mode’ where NO (500 ppmv in N₂) was added in addition to the CO flow to convert all
242 RO₂ into OH before all OH was then rapidly converted by CO into HO₂. The air from the
243 RO_xLIF reactor was then drawn into the FAGE low pressure fluorescence cell, whereupon pure



244 NO (Messer, 99.5 %) was injected to convert HO₂ to OH. In HO_x mode, the sum of OH, HO₂
245 and complex RO₂ was measured, while in RO_x mode, the sum of OH, HO₂ and total RO₂ was
246 measured. From this the concentration of complex RO₂ and HO₂/OH from RO_x can be
247 determined.

248 An Inlet Pre-Injector was used attached to the HO_x cell to remove ambient OH by injecting
249 propane directly above the inlet of the cell. This leads to a background measurement while the
250 laser is still online to the OH transition; this background is known as OH_{CHEM}. OH_{CHEM} includes
251 signal from laser scatter and scattered solar radiation and any fluorescence signal from any OH
252 generated inside the cell from an interference precursor. By comparing OH_{CHEM} to the signal
253 generated when the 308 nm laser tuned off the OH transition, OH_{WAVE}, the contribution of any
254 interference can be identified. While the laser is offline, OH_{WAVE}, any signal seen is from laser
255 scattered light and scattered solar radiation. Agreement between OH_{WAVE} and OH_{CHEM} was
256 generally very good during the Summer AIRPRO campaign with an overall orthogonal
257 distance regression slope of 1.103 ± 0.017 , with the exception of an interference seen when O₃
258 levels were elevated (see Woodward-Massey et al., 2020 for details).

259 **2.3 Determination of aerosol soluble copper concentration through ICP- 260 MS Analysis**

261 The soluble copper ion concentration was determined by analysing the effluent extracted from
262 quartz filter samples taken daily for the entire campaign using Inductively Coupled Plasma
263 Mass Spectrometry (ICP-MS). A 6 cm² punch from each large quartz filter PM_{2.5} sample was
264 cut and put in a 15 mL extraction tube and extracted with 10 mL ultrapure water (18.2 MΩ
265 cm) under ultrasonication for 60 minutes at below 35 °C. The sample was then shaken by a
266 temperature-controlled shaker at 4 °C for 3 hours at approximately 60 cycles min⁻¹. After
267 filtering through a filter syringe, 8 mL of effluent was transferred to a new 15 mL metal free
268 tube, and 2 mL of 10% HNO₃ was added to make a 10 mL 2% HNO₃ extract solution which
269 was then analysed to determine the soluble copper ion concentration using ICP-MS.

270 **2.4 MCM v3.3.1 box model description**

271 The Master Chemical Mechanism (MCMv3.3.1) is a near-explicit mechanism which describes
272 the gas-phase degradation of a series of primary emitted VOC's in the troposphere. The
273 mechanism considers the degradation of 143 VOC's and contains ~17000 elementary reactions
274 of 6700 species (Whalley et al., 2013).



275 The model was constrained to measurements of NO, NO₂, O₃, CO, HCHO, HNO₃, HONO,
276 PAN, H₂O vapour, temperature, pressure, $j(\text{O}^1\text{D})$, $j(\text{HONO})$, $j(\text{NO}_2)$, $j(\text{ClONO}_2)$, $j(\text{HOCl})$,
277 $j(\text{ClONO}_2)$ and specific VOC species measured using GC-FID (gas chromatography with
278 flame ionisation) and PTR-ToF-MS (proton-transfer reaction time of flight mass
279 spectrometry). The measured species were input into the model at a time resolution of 15
280 minutes, with species measured at a higher time resolution averaged up to 15 minutes and those
281 measured at a lower time resolution interpolated to give a value every 15 minutes. The full list
282 of all species constrained in the model is shown in Table 1.

Type	Species
Gas-phase inorganic species	NO, NO ₂ , O ₃ , CO, HNO ₃ , HONO, H ₂ O, SO ₂ , ClONO ₂ , HOCl
Gas-phase organic species	HCHO, PAN, CH ₄ , C ₂ H ₆ , C ₂ H ₄ , C ₃ H ₈ , C ₃ H ₆ , isobutane, butane, C ₂ H ₂ , trans-but-2-ene, but-1-ene, Isobutene, cis-but-2-ene, 2-Methylbutane, pentane, acetone, 1,3-butadiene, trans-2-pentene, cis-2-pentene, 2-methylpentane, 3-methylpentane, hexane, isoprene, heptane, benzene, toluene, nonane, decane, undecane, dodecane, o-xylene, CH ₃ OH, CH ₃ OCH ₃ , 2-ethyltoluene, 3-ethyltoluene, 4-ethyltoluene, ethylbenzene, CH ₃ CHO, C ₂ H ₅ OH, α -pinene, limonene, isopropylbenzene, propylbenzene, m-xylene, p-xylene, 1,2,3-trimethylbenzene, 1,2,4-trimethylbenzene, 1,3,5-trimethylbenzene.
Photolysis rates	$j(\text{O}^1\text{D})$, $j(\text{HONO})$, $j(\text{NO}_2)$, $j(\text{ClONO}_2)$, $j(\text{HOCl})$, $j(\text{ClONO}_2)$
Other	Mixing height, aerosol surface area

283 **Table 1.** Full description of measured species during Summer AIRPRO campaign constrained within the model

284 The different model scenarios referred to in this study are described in full below:

- 285 1. **MCM_base:** The base model run constrained to species described in Table 1.
- 286 2. **MCM_gamma:** The base model including heterogeneous HO₂ uptake onto
287 aerosols with γ_{HO_2} calculated from parameterisation developed by Song et al., 2020.
- 288 3. **MCM_SA:** The base model including heterogeneous HO₂ uptake, this time with
289 γ_{HO_2} fixed at 0.2, as commonly used within models and recommended by Jacob,
290 2000.



291 2.5 Description of the “Song parameterisation”

292 A large uncertainty in determining the effect of HO₂ uptake onto the surface of aerosol particles
293 is the lack of understanding of the dependence of γ_{HO_2} on Cu (II)/transition metal ion
294 concentration within aerosols. Experimentally this dependence is quite well known from
295 laboratory studies (Mozurkewich et al., 1987; Thornton and Abbatt, 2005; George et al., 2013;
296 Mao et al., 2013), however the effective concentrations in ambient aerosols and the impact on
297 γ_{HO_2} of aerosol liquid water concentration, [ALWC], has not been incorporated into models
298 before. A novel parameterisation was developed by Song et al., 2020 in the framework of the
299 resistor model to include the influence of aerosol soluble copper on the uptake of HO₂. The
300 new parameterisation for the uptake coefficient of HO₂ onto aerosols, as given in Song et al.,
301 2020, is as follows:

$$\frac{1}{\gamma_{HO_2}} = \frac{1}{\alpha_{HO_2}} + \frac{3 \times v_{HO_2}}{(4 \times 10^6) \times R_d H_{eff} RT \times \left(5.87 + 3.2 \ln \left(\frac{ALWC}{[PM] + 0.067} \right) \right) \times [PM]^{-0.2} \times [Cu^{2+}]_{eff}^{0.65}} \quad (1)$$

302 where γ_{HO_2} is the uptake coefficient of HO₂ onto aerosols, α_{HO_2} is the mass accommodation
303 coefficient of HO₂, v_{HO_2} is the mean molecular speed in cm s⁻¹, R_d is the count median radius
304 of the aerosol in cm, H_{eff} is the effective Henry’s Law constant calculated from $H_{eff} =$
305 $H_{HO_2} \left(1 + \frac{K_{eq}}{[H^+]} \right)$ where H_{HO_2} is the physical Henry’s Law constant for HO₂ (i.e. 3900
306 (Thornton et al., 2008)) in M atm⁻¹, K_{eq} is the equilibrium constant for HO₂ dissociation (M),
307 and $[H^+]$ is the hydrogen ion concentration within the aerosol calculated from the pH (M), R
308 is the gas constant in cm³ atm K⁻¹ mol⁻¹ (i.e. 82.05), T is the temperature in K, [ALWC] is the
309 aerosol liquid water content in µg m⁻³ (which is related to the ambient relative humidity), [PM]
310 is the mass concentration of PM_{2.5} in µg m⁻³ and $[Cu^{2+}]_{eff}$ is the effective aerosol condensed-
311 phase soluble copper (II) ion concentration in mol L⁻¹.

312 The Song parameterisation can reportedly be used for urban environmental conditions of
313 aerosol mass concentrations between 10-300 µg m⁻³; aqueous copper (II) concentrations of
314 10⁻⁵–1 mol L⁻¹; and relative humidity between 40-90 %. However, for the Summer AIRPRO
315 campaign data, the minimum [ALWC] supported by the parameterisation was 14 µg m⁻³, below
316 which the parameterisation returned negative values for γ_{HO_2} . As such, despite the average
317 calculated [ALWC] for the campaign being 6.9 ± 10 µg m⁻³, a fixed value of 14 µg m⁻³ was
318 used to calculate γ_{HO_2} across the entire campaign.



319 **3 Results and Discussion**

320 **3.1 Overview of field observations during summer AIRPRO campaign**

321 Radical concentration measurements were taken throughout the official science period of the
322 summer campaign, from 23/05/2017 to 22/06/2017, using the Fluorescence Assay by Gas
323 Expansion technique. Alongside the radical observations and photolysis rate measurements
324 made by the University of Leeds, there was a varied suite of supporting measurements operated
325 by several universities and institutions. The supporting measurements used for the analysis and
326 discussion in this study were provided chiefly by the Universities of York, Birmingham and
327 Cambridge as detailed in Table 2.

328

329

330

331

332

333

334

335

336

337

338

339

340

341

342

343



Instrument	Species measured	University	Reference
FAGE	OH, HO ₂ , RO ₂	Leeds	Whalley et al., 2010; Whalley et al., 2021; Slater et al., 2020
OH reactivity	OH reactivity	Leeds	Stone et al., 2016; Whalley et al., 2021; Slater et al., 2020
Spectral Radiometer	Photolysis rates	Leeds	Bohn et al., 2016
Filter Radiometer	<i>j</i> (O ¹ D)	Leeds	Whalley et al., 2010
Teledyne CAPS	NO ₂	York	Smith et al., 2017
TEI 42c	Total NO _y	York	Smith et al., 2017
TEI 49i	O ₃	York	Smith et al., 2017
Sensor box	CO	York	Smith et al., 2017
DC-GC_FID	C ₂ -C ₇ VOCs and oVOCs	York	Hopkins et al., 2011
GCxGC-FID	C ₆ -C ₁₃ VOCs and oVOCs	York	Dunmore et al., 2015
BBCEAS	HONO	Cambridge	Le Breton et al., 2014
TEI 42i	NO	Birmingham	-
LOPAP	HONO	Birmingham	Crilley et al., 2016
SMPS	Particle Size distribution	Birmingham	Wiedensohler et al., 2012
High volume sampler	PM _{2.5} filter samples, Aerosol copper	IAP	-

344 **Table 2.** Measurements taken by universities and institutions during the Beijing Summer AIRPRO campaign.
345 These species are directly referred to in this chapter: full description of every instrument and measurement taken
346 can be found in Slater, 2020. IAP: Institute of Atmospheric Physics, Beijing. Time resolution of all instruments
347 was averaged up to or interpolated down to 15 minutes for modelling purposes with the exception of the PM_{2.5}
348 filter samples, of which there was only 1 sample taken a day.

349 The median average diurnals for important gas phase species (ppb) and *j*(O¹D) (s⁻¹) measured
350 during the summer campaign are shown in Figure 1. *j*(O¹D) showed a maximum at solar noon
351 peaking at $2.5 \times 10^{-5} \text{ s}^{-1}$. The diurnal variation in both NO and NO₂ was very distinct, with a
352 peak in NO at rush hour (~08:00) of ~ 8 ppb. NO decreased into the afternoon following this
353 morning peak to a minimum of 0.3 ppb. The low values of NO mixing ratio observed in the
354 afternoon were a result of high levels of O₃, peaking at 89 ppb at ~15:30, leading to increased
355 titration of NO + O₃ to give NO₂, the diurnal of which can be seen to peak in the morning at
356 ~ 32 ppb at 06:30, coinciding with peak in traffic emissions. Conversely O₃ mixing ratio was
357 at a minimum of ~14 ppb during the morning traffic peak in NO. Due to the expected



358 accumulation of HONO overnight, HONO mixing ratio is highest in the morning, peaking
359 before 07:30 at ~ 7 ppb, after which HONO is lost rapidly via photolysis to give OH + NO.
360 This study will use these measured observations to compare modelled and measured
361 concentrations of OH, HO₂ and RO₂ radicals and investigate the effect of HO₂ uptake on radical
362 concentrations.

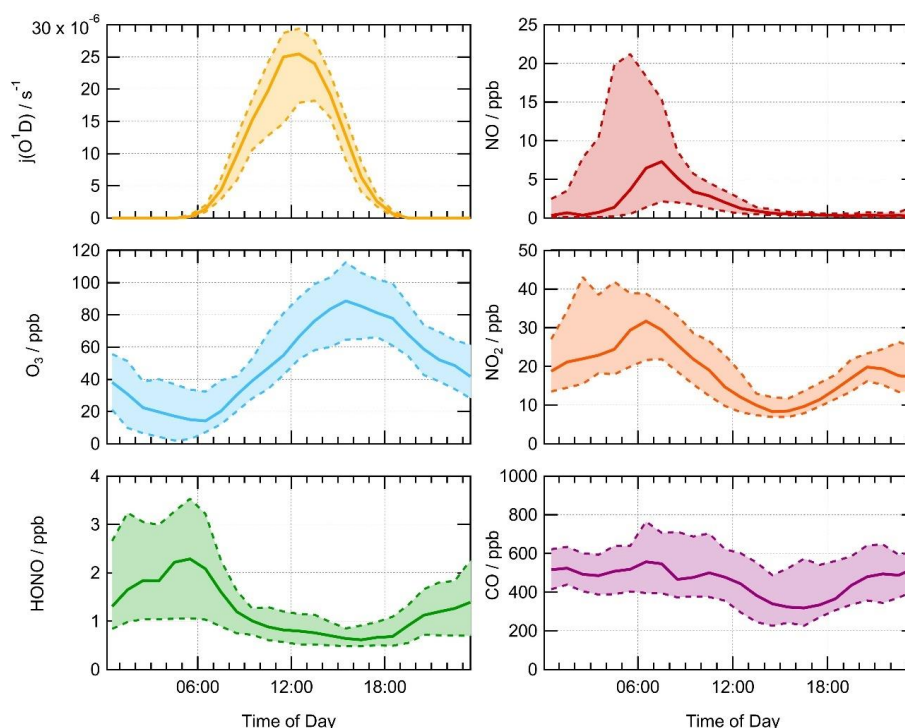


Figure 1. Average median diurnal profile for measured $j(\text{O}^1\text{D})$ (s^{-1}), O_3 (ppb), HONO (ppb), NO (ppb), NO_2 (ppb) and CO (ppb) for the Summer AIRPRO campaign. The dashed lines with shaded regions represent the 25th/75th percentiles. Diurnals show 60 minute averages, taken over the entire measurement period.

363 The majority of the Summer Beijing campaign occurred during a non-haze period, meaning
364 $\text{PM}_{2.5}$ concentrations remained below $75 \mu\text{g m}^{-3}$, only exceeding this on the 28/05, 31/05,
365 05/06, 07/06, 17/06 and 18/06/2017. The average median diurnal of $\text{PM}_{2.5}$ surface area
366 ($\text{cm}^2 \text{cm}^{-3}$) is shown in Figure 2. $\text{PM}_{2.5}$ surface area concentration was available at a higher
367 resolution due to use of online particle sizers compared to filter samples taken daily to give
368 $\text{PM}_{2.5}$ mass concentration. $\text{PM}_{2.5}$ surface area was then averaged up to a time resolution of 15
369 minutes to be used in the model. No strong diurnal trend was seen, with an average across the
370 campaign of $5.5 \times 10^{-6} \text{cm}^2 \text{cm}^{-3}$, with a maximum surface area of $2.5 \times 10^{-5} \text{cm}^2 \text{cm}^{-3}$.

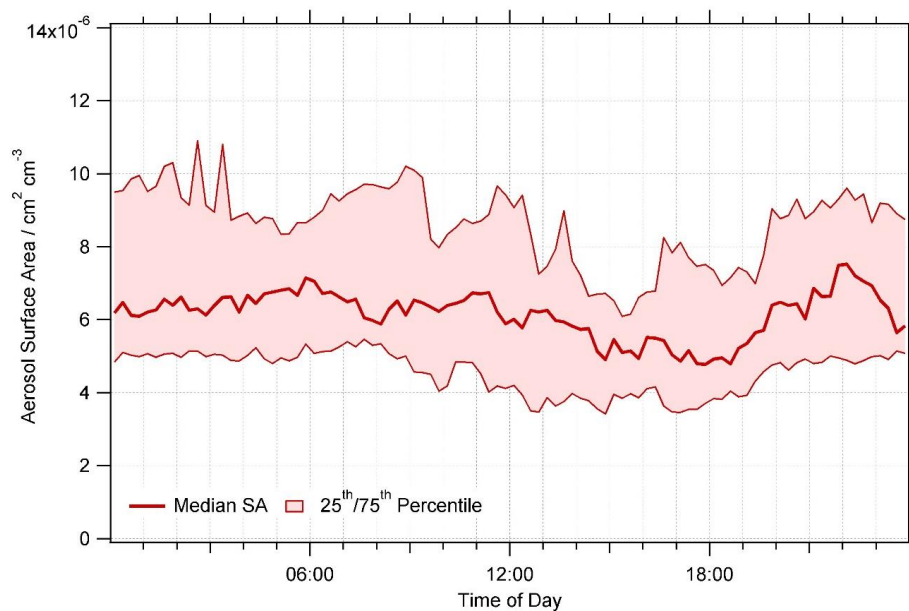


Figure 2. Average median diurnal of $\text{PM}_{2.5}$ aerosol surface area ($\text{cm}^2 \text{cm}^{-3}$) for Summer AIRPRO campaign. Data averaged up to 15 mins time resolution. The dashed lines with shaded regions represent the 25th/75th percentiles.

371 During haze periods in Beijing, it is expected that a strong correlation would exist between
372 $\text{PM}_{2.5}$ and NO_x , as seen in Winter Beijing AIRPRO campaign in 2016 (Slater et al., 2020).
373 However, during the Summer campaign, no strong correlation between $\text{PM}_{2.5}$ and NO_x was
374 seen. The time series of NO (ppb) and $\text{PM}_{2.5}$ ($\text{cm}^2 \text{cm}^{-3}$) is shown in Figure 3. A correlation
375 plot of $\text{PM}_{2.5}$ aerosol surface area ($\text{cm}^2 \text{cm}^{-3}$) versus NO and NO_2 mixing ratio (ppb) is shown
376 in Figure 1 of Supplementary Information.

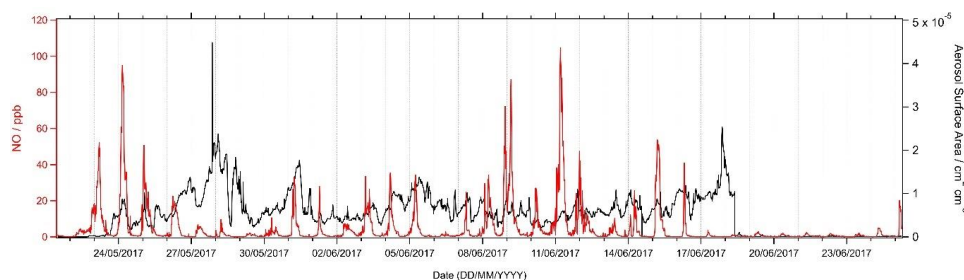


Figure 3. Time series of measured NO / ppb and $\text{PM}_{2.5}$ / $\text{cm}^2 \text{cm}^{-3}$ across entire summer AIRPRO campaign in Beijing.



377 **3.2 Calculated γ_{HO_2} for summer AIRPRO campaign**

378 Measured values of [PM], copper (II) ion concentration and aerosol pH (used to calculate H_{eff}
379 in equation 1), and values of [ALWC] estimated using the ISORROPIA-II thermodynamic
380 equilibrium model (Fountoukis and Nenes, 2007) were input into the parameterisation at a time
381 resolution of 1 day. $PM_{2.5}$ mass concentration and Cu (II) ion concentration values were
382 measured by extracting from filter samples offline with one filter sample taken every day. As
383 such all measured values input into the parameterisation were averaged up to this time
384 resolution. R_d was calculated from the measured aerosol size distribution across the entire
385 campaign. A value of 0.5 was chosen for the mass accommodation coefficient, α_{HO_2} , to reflect
386 values previously measured for copper doped inorganic salts (Thornton and Abbatt, 2005;
387 George et al., 2013; Taketani et al., 2008) and to allow better comparison with results from
388 Song et al., 2020. For summer AIRPRO campaign, the soluble copper ion concentration was
389 measured by extracting Cu (II) ions from filter samples and analysing the effluent using
390 Inductively Coupled Plasma Mass Spectrometry (ICP-MS). As in Song et al., 2020, the total
391 copper (II) mass concentration ($ng\ m^{-3}$ converted to $g\ m^{-3}$) was divided by the aerosol volume
392 concentration ($nm^3\ cm^{-3}$ converted to $dm^3\ m^{-3}$) and the molar mass of copper ($g\ mol^{-1}$) to give
393 the total copper molar concentration in the aerosol, $[Cu^{2+}]_{eff}$ ($mol\ L^{-1}$), which was then used in
394 equation 1. The average values across summer AIRPRO campaign for parameters used in
395 equation 1 are shown in Table 3.

Parameter	Average value across campaign
Temperature (K)	300
Relative humidity (%)	43
Aerosol pH	3
Count median radius (cm)	2.3×10^{-6}
ALWC ($\mu g\ m^{-3}$) ^a	14
[PM] ($\mu g\ m^{-3}$)	38.3
$[Cu^{2+}]_{eff}$ ($mol\ L^{-1}$)	0.0008
$[Cu^{2+}]_{eff}$ ($ng\ m^{-3}$)	4
α_{HO_2}	0.5 (fixed)

396 **Table 3.** Average values for summer AIRPRO campaign in Beijing, 2017 for parameters in equation 1. ^aThis was
397 a fixed minimum value of ALWC for the parameterisation to be used for this data set, fully explained in Section
398 3.4. Cu (II) ion concentration is given in both $mol\ L^{-1}$ and $ng\ m^{-3}$, due to $mol\ L^{-1}$ being used in equation 1 but ng
399 m^{-3} being the more atmospherically relevant unit.



400 For the Beijing summer AIRPRO campaign, an average value of $\gamma_{HO_2} = 0.07 \pm 0.035$ (1σ) was
401 calculated across the entire campaign, with values ranging from 0.002 to 0.15. The time series
402 for the calculated γ_{HO_2} , R_d (cm), [PM] ($\mu\text{g m}^{-3}$), [ALWC] ($\mu\text{g m}^{-3}$) and $[\text{Cu}^{2+}]_{\text{eff}}$ (mol L^{-1}) is
403 shown in Figure 4.

404 As fully described in Song et al., 2020 supplementary information, the uncertainty in the
405 calculation of γ_{HO_2} using equation 1 comes mainly from the uncertainty in [ALWC] (~ 10 - 20
406 %, calculated using ISORROPIA-II (Fountoukis and Nenes, 2007)), the uncertainty in the mass
407 accommodation coefficient (varying a_{HO_2} within the parameterisation from 0.1 to 1, increased
408 the calculated γ_{HO_2} from 0.042 to 0.077. However, by $a_{HO_2} = 0.5$ this dependence has begun to
409 plateau with $\gamma_{HO_2} = 0.070$ when $a_{HO_2} = 0.5$), and the uncertainty of the model calculations used
410 to formulate the parameterisation (~ 40 % as explained in Song et al., 2020). Uncertainties in
411 measured parameters i.e. temperature, [PM], $[\text{Cu}^{2+}]$ and count median radius are due to
412 associated instrumental error which are assumed small in comparison.

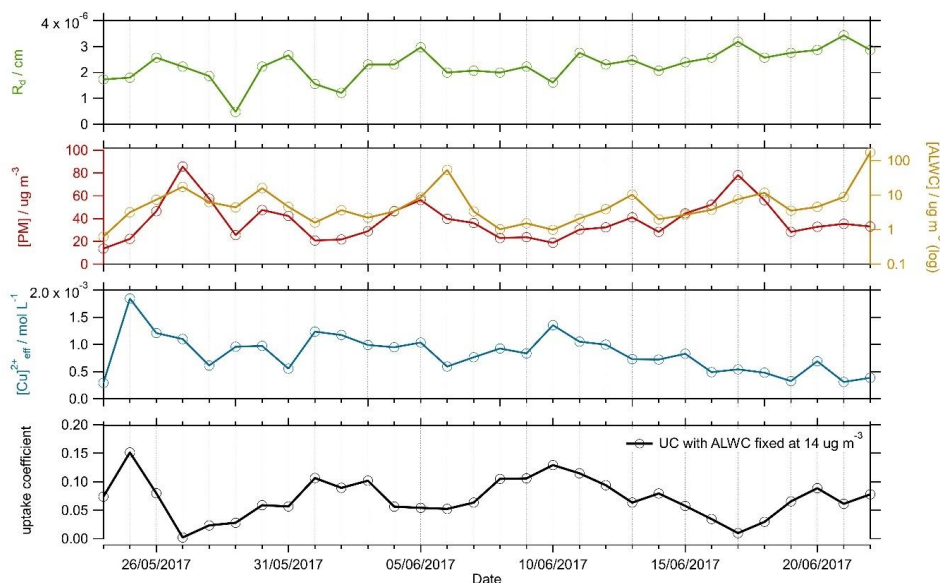


Figure 4. Time series of R_d (cm, orange), [PM] ($\mu\text{g m}^{-3}$, red), [ALWC] ($\mu\text{g m}^{-3}$, yellow) and $[\text{Cu}^{2+}]_{\text{eff}}$ (mol L^{-1} , blue), parameters used in equation 1 to calculate γ_{HO_2} (bottom panel). Each parameter has been averaged up to a time resolution of 1 day to match the lowest resolution measurement. The calculated γ_{HO_2} is shown in the bottom panel, for a fixed [ALWC] = $14 \mu\text{g m}^{-3}$ (solid black line).

413 To examine the effect within the Song parameterisation of [PM] and [ALWC] on γ_{HO_2} as a
414 function of copper molarity, the uptake coefficient was calculated by varying the $[\text{Cu}^{2+}]_{\text{eff}}$



415 concentration within the parameterisation with alternatively fixed values of [PM] or [ALWC].
416 For a given value of $[\text{Cu}^{2+}]_{\text{eff}}$, at fixed [ALWC] an increase in [PM] causes a decrease in the
417 curvature of γ_{HO_2} vs $[\text{Cu}^{2+}]_{\text{eff}}$, whereas at a fixed [PM], an increase in [ALWC] leads to an
418 increase in γ_{HO_2} for a given $[\text{Cu}^{2+}]_{\text{eff}}$. As shown in Figure 5, [ALWC] and [PM] have the
419 greatest effect on γ_{HO_2} between $[\text{Cu}^{2+}]_{\text{eff}} = 10^{-5}$ - 10^{-1} M before the curve levels off towards the
420 mass accommodation coefficient of 0.5, as input into the model. For context within the Beijing
421 campaign, the curve of γ_{HO_2} vs $[\text{Cu}^{2+}]_{\text{eff}}$ was plotted in Figure 5 using the average values for
422 the AIRPRO summer campaign fixed at [ALWC] = 14 ug m^{-3} and [PM] = 38.3 ug m^{-3} . For the
423 average AIRPRO summer campaign values, an increase $[\text{Cu}^{2+}]_{\text{eff}}$ has the most effect on γ_{HO_2}
424 between $[\text{Cu}^{2+}]_{\text{eff}} \sim 10^{-3}$ - 10^{-1} M, with the average $[\text{Cu}^{2+}]_{\text{eff}}$ for the campaign being 8×10^{-4} M
425 (values ranged from 3×10^{-4} to 2×10^{-3} M across campaign).

426

427

428

429

430

431

432

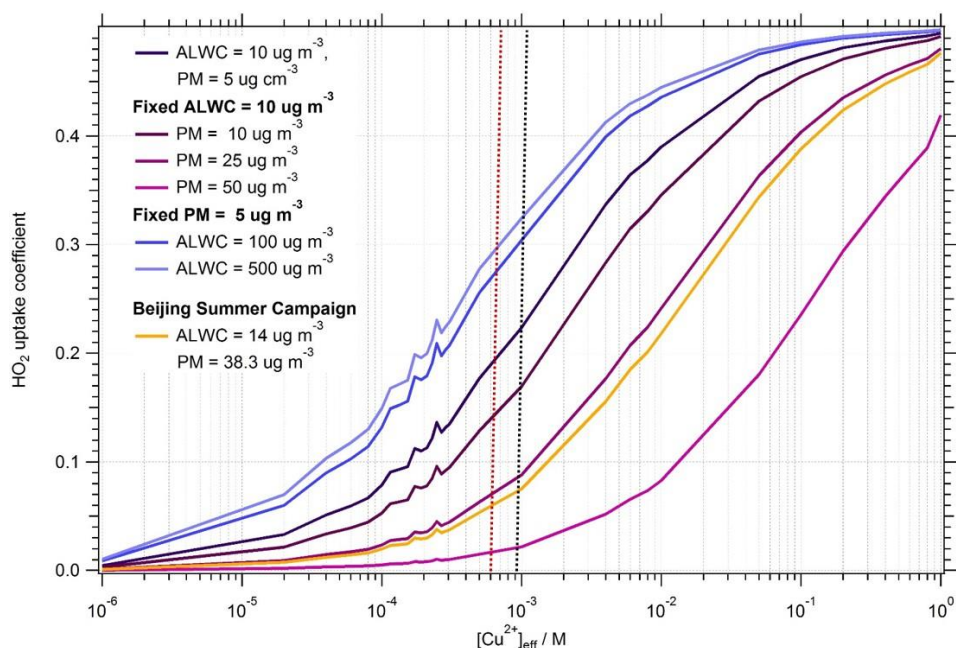


Figure 5. Dependence of uptake coefficient, γ_{HO_2} on aerosol copper concentration, $[Cu^{2+}]_{eff}$ (M), showing the effect of varying [PM] with fixed [ALWC] and vice versa. Pink to purple lines show the effect on uptake coefficient of varying [PM] from 5–50 $\mu\text{g m}^{-3}$ with a fixed [ALWC] of 10 $\mu\text{g cm}^{-3}$. Blue to dark blue lines show the effect on γ_{HO_2} of varying [ALWC] from 10–500 $\mu\text{g m}^{-3}$ (much higher than typically seen atmospherically) with a fixed [PM] of 5 $\mu\text{g m}^{-3}$. The yellow line shows the effect on the γ_{HO_2} of varying $[Cu^{2+}]_{eff}$, with [ALWC] and [PM] taken as the averages from the Beijing campaign, i.e. [ALWC] = 14 $\mu\text{g m}^{-3}$ and [PM] = 38.8 $\mu\text{g m}^{-3}$. Black dashed line indicates the average $[Cu^{2+}]_{eff}$ for Beijing summer campaign. Red dashed line indicates the average $[Cu^{2+}]_{eff}$ for the Wangdu campaign. Note that the [PM] and [ALWC] are both higher for Wangdu campaign compared to the Beijing campaign.

433 3.3 Box modelling results

434 3.3.1 Effect of calculated γ_{HO_2} on modelled AIRPRO Summer radical concentrations

435 As reported in Whalley et al., 2021, radical concentrations were high during the AIRPRO
436 summer campaign with maximum measured concentrations of OH, HO₂ and RO₂ of 2.8×10^7
437 molecule cm^{-3} , 1×10^9 molecule cm^{-3} and 5.5×10^9 molecule cm^{-3} on the afternoons of the
438 30th May, 9th June and 15th June respectively. The time series of measured OH, HO₂ and RO₂
439 for the entire summer campaign as measured by the Leeds FAGE instrument with MCM_base
440 model outputs for OH, HO₂ and RO₂ can be found in Whalley et al., 2021. Using the MCM
441 and the γ_{HO_2} calculated for the Summer Beijing campaign with the Song parameterisation, the



442 effect of HO₂ uptake on the concentration of OH, HO₂ and RO₂ radicals was investigated and
443 compared to the base model.

444 The MCM_base model predicted radical concentrations are shown as average diurnal profiles
445 compared to both the measured diurnals and the MCM_gamma model in Figure 6. A detailed
446 description of the diurnal variation in measured and modelled OH, HO₂ and RO₂ radicals for
447 the summer Beijing campaign is given in Whalley et al., 2021, so only a brief summary will be
448 given here.

449 The average diurnal profiles show that the MCM_base model can re-produce the measured OH
450 concentrations relatively well, however the modelled peak in OH is shifted to the afternoon
451 with a peak at ~14:00 compared to the midday peak in the observations. In comparison, HO₂
452 is over-predicted, particularly during the day with the exception being when NO was high from
453 9-12th June. Day-time HO₂ is over-predicted on average by MCM_base by up to a factor of
454 ~2.9 with a peak in the diurnal at ~ 14:30. In-comparison, daytime RO₂ concentration is under-
455 predicted on average by MCM_base by up to a factor of ~7.5, with a larger under-prediction
456 in the morning between ~6:30-10:30 when NO levels were highest. At the peak of the RO₂
457 diurnal, on average the concentration was under-predicted by MCM_base by a factor of ~2.7.
458 While the MCM_base model is able to reproduce measured OH concentrations reasonably
459 well, the inability of this model to reproduce HO₂ and RO₂ suggests missing key reactions. In
460 Whalley et al., 2021, budget analysis highlighted a missing source of OH, in addition to a
461 missing RO₂ production reaction which could partially explain the under-prediction of RO₂ by
462 the MCM_base model. It was also suggested that the over-prediction of HO₂ could be due, in
463 part, to an under-prediction in the rate of reaction of RO₂ with NO to produce a different RO₂
464 species, i.e. RO₂+NO→RO₂' , which would lead to propagation of RO₂ to different, more
465 oxidised RO₂ species, competing with the recycling of RO₂ via RO to give HO₂, or due to lack
466 of RO₂ autoxidation pathways within the model which could lead to the formation of highly
467 oxygenated molecules as opposed to HO₂. The higher measured RO₂ concentrations could,
468 therefore, suggest that the lifetime of total RO₂ is longer than currently considered in the model.

469 As stated in Section 3.3, for the Beijing summer AIRPRO campaign, values of calculated γ_{HO_2}
470 varied ranging from 0.002 to 0.15, giving an average value of $\gamma_{HO_2} = 0.07 \pm 0.035$ (1 σ) across
471 the campaign. These γ_{HO_2} values calculated on a daily time resolution, were added into the
472 MCM_base model to give the MCM_gamma model. The average median diurnals of modelled



473 OH, HO₂ and RO₂ (molecule cm⁻³) for MCM_base, MCM_gamma (with γ_{HO_2} ranging from
474 0.002-0.15) and MCM_SA (with γ_{HO_2} fixed at 0.2) are shown in Figure 6.

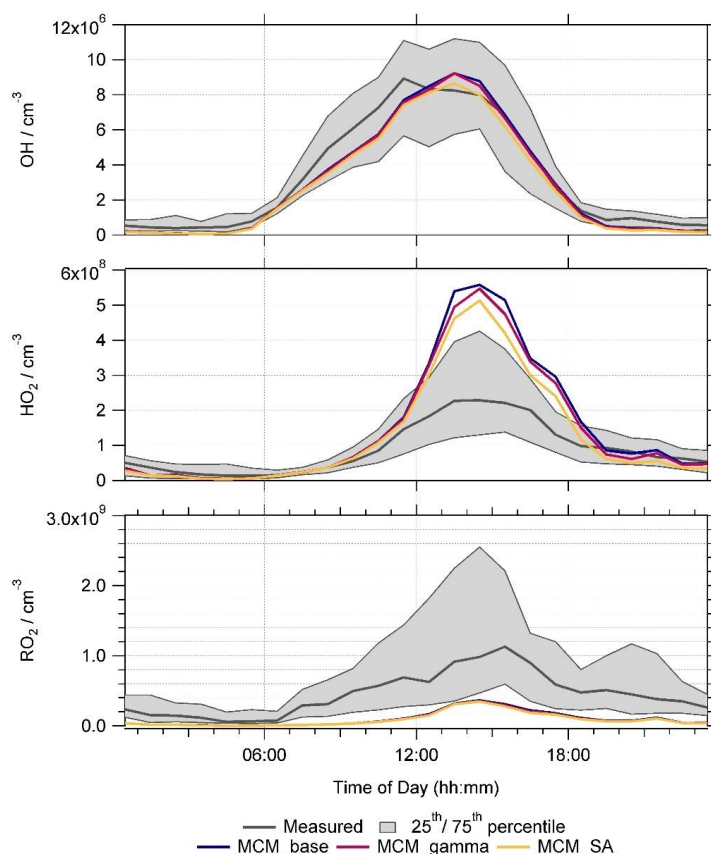


Figure 6. Average median diurnals for measured radical concentrations (grey) and modelled OH, HO₂ and total RO₂ radical concentrations in molecule cm⁻³ for MCM_base (blue), MCM_gamma (dark pink) and MCM_SA (yellow) model runs. All diurnal's are 60 minute averages, taken over the entire measurement period. Shaded grey regions represent the 25th/75th percentiles of measured radical data.

475 Due to a combination of the calculated uptake coefficient being smaller, on average, than
476 usually used within models (i.e < 0.2), and the high NO_x levels, little effect on average radical
477 diurnals was seen by adding in HO₂ aerosol uptake into the model. Figure 6 shows that the OH
478 and RO₂ radical concentrations were not significantly affected on average across the campaign
479 by the addition of aerosol uptake. The average median diurnal of HO₂ can be seen as slightly
480 decreased, i.e. the over-prediction of HO₂ is slightly less for MCM_gamma compared to
481 MCM_base, with the over-prediction decreasing from a factor of ~ 2.9 to ~ 2.4 at the 14:30 peak
482 in the diurnal.



483 Due to the recycling of RO_2 to HO_2 and then back to OH by NO, it is important to consider the
484 dependency of radicals on NO and whether the addition of the HO_2 uptake coefficient has an
485 effect on the model's ability to predict the dependency of radical concentrations on NO. The
486 dependency of measured/modelled OH, HO_2 and RO_2 on NO mixing ratio is discussed fully
487 for the MCM_base model in Whalley et al., 2021. Figure 7 shows the ratio of measured to
488 modelled OH, HO_2 and RO_2 radical concentrations binned against NO mixing ratio (ppb) for
489 MCM_gamma, compared to MCM_base.

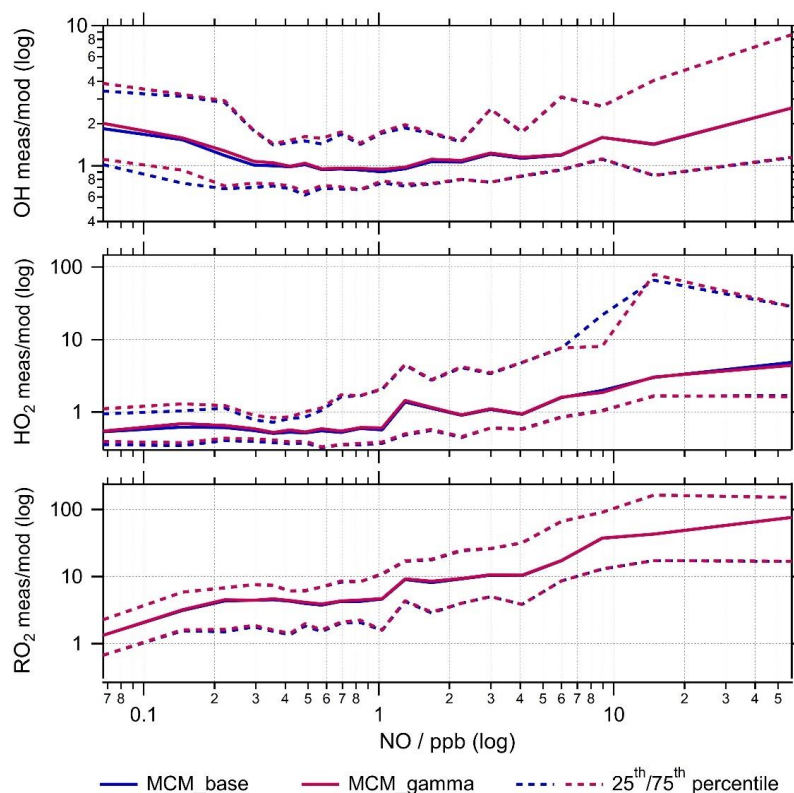


Figure 7. Ratio of measured to modelled OH, HO_2 and RO_2 radical concentrations using the MCM_base (blue) and MCM_gamma (dark pink) model binned over the range of NO mixing ratios (ppb) for the summer AIRPRO campaign. Solid lines show the median average measured to modelled radical concentration. Dashed lines show the 25th/75th percentiles.

490 For the range of NO mixing ratios observed across the summer AIRPRO campaign, the OH
491 measured to modelled ratio is close to 1 between ~0.3 and 2 ppb NO with the MCM_base
492 model beginning to under-predict OH slightly both below 0.3 ppb NO and above 2 ppb NO.
493 Both HO_2 and RO_2 radical concentrations were strongly dependent on NO mixing ratio, with



494 the model over-predicting HO₂ below ~ 1 ppb NO. For the entire campaign the average NO
495 was 4.7 ppb with 45% of NO measurements taken across campaign being less than or equal to
496 1 ppb. Across all NO mixing ratios the measured to modelled ratio for RO₂ shows a large
497 under-prediction, with the largest under-prediction at the highest NO mixing ratios. This is
498 likely contributing to the underprediction of HO₂ at higher NO mixing ratios. From Figure 7 it
499 can be seen that the addition of the calculated HO₂ uptake coefficient has had little effect across
500 the range of NO mixing ratios measured during the summer AIRPRO campaign.

501 To showcase any effect adding HO₂ aerosol uptake would have on HO₂ loss pathways as a
502 whole, and thereby make a judgement on the effect of decreased PM_{2.5} and hence HO₂ loss via
503 aerosol surfaces on the O₃ production within Beijing, a rate of destruction analysis (RODA)
504 was done for MCM_gamma. The loss pathways of HO₂ within MCM_gamma are shown in
505 Figure 8 as an average median diurnal and as a function of NO mixing ratio (ppb), in addition
506 to the percentage contribution of HO₂ uptake to the overall loss of HO₂ within the model.

507

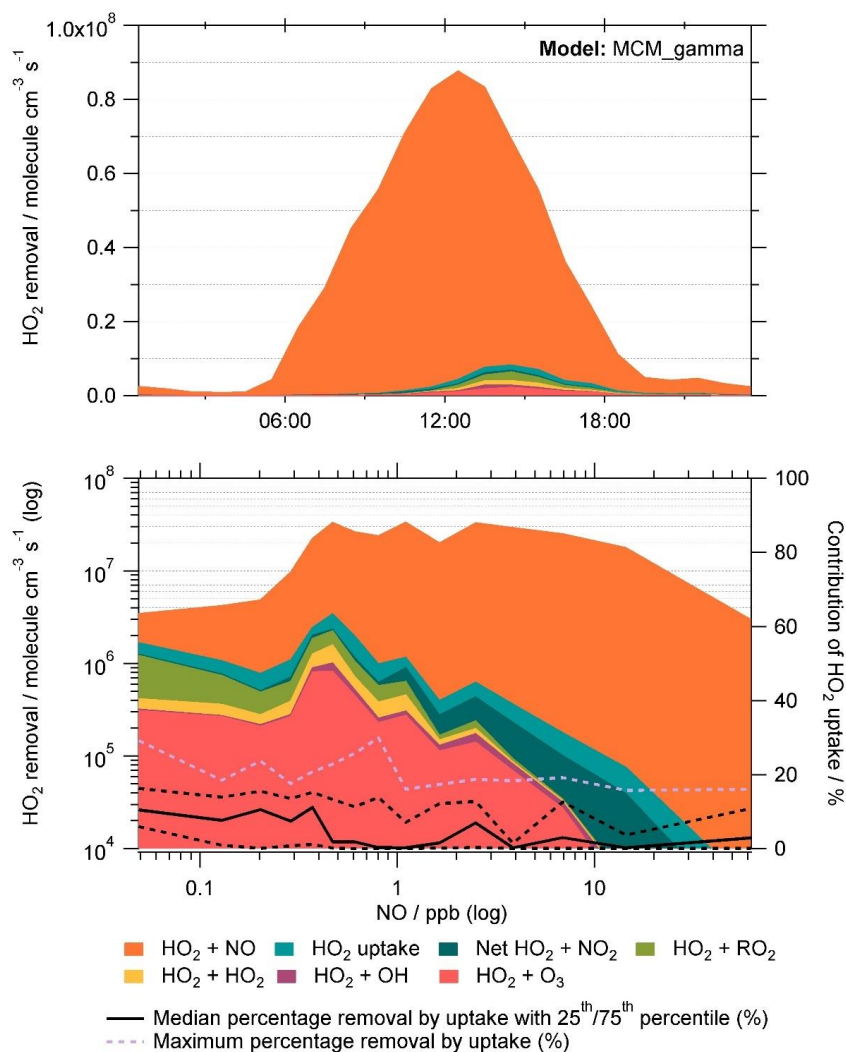


Figure 8. Rate of destruction analysis (RODA) showing the dominant loss pathways of HO₂ within MCM_gamma shown as (a) a diurnal variation and (b) as a function of NO mixing ratio (ppb). Median removal of HO₂ by uptake (%) as a function of NO (ppb) is shown as solid black line in (b), with 25th/75th percentile shown as the black dashed lines. Maximum percentage removal by uptake for a given NO mixing ratio is shown as a lilac dashed line.

508 As shown in the RODA, the dominant loss pathway of HO₂ is HO₂ + NO across the entire
 509 campaign (90 ± 14 % of total loss), followed by HO₂ + RO₂ (3.5 ± 8.1 % of total loss). This is
 510 expected due to high levels of NO_x in Beijing, especially during the day. As seen in the RODA
 511 diurnal, the HO₂ + NO loss pathway peaks at midday following the morning peak in NO mixing
 512 ratio due to rush hour traffic. As NO mixing ratio decreases, the relative importance of other



513 loss pathways of HO₂ increases. At the lowest NO mixing ratio, i.e. < 0.1 ppb NO, the loss
514 pathways of HO₂ within MCM_gamma with the largest contribution to total loss were HO₂ +
515 NO (55 ± 19 %), HO₂ + RO₂ (23 ± 17 %) and HO₂ + O₃ (9.3 ± 4.1 %). It is worth noting that
516 as the NO mixing ratio decreases the relative importance of HO₂ removal by O₃ increases
517 presumably due to the titration reaction of O₃ with NO decreasing (and hence higher observed
518 [O₃]). This could be important when considering policy changes with NO_x pollution in China
519 decreasing in recent years. The contribution of the various loss pathways of HO₂ to total HO₂
520 loss within MCM_gamma under low (< 0.1 ppb) and high (>0.1 ppb) NO are compared in
521 Table 4.

	HO ₂ +O ₃	HO ₂ +OH	HO ₂ +HO ₂	HO ₂ +RO ₂	Net HO ₂ +NO ₂	HO ₂ +NO	uptake
Low NO (< 0.1 ppb)	9.3 ± 4.1	0.1 ± 0.1	3.0 ± 1.8	23 ± 17	2.4 ± 3.0	55 ± 19	7.3 ± 7.3
High NO (> 0.1 ppb)	1.8 ± 2.3	0.2 ± 0.3	0.8 ± 1.3	2.0 ± 4.4	0.4 ± 1.2	93 ± 9.0	1.9 ± <0.01

522 **Table 4.** Average relative percentage contribution of individual HO₂ loss pathways to the total loss of HO₂ within
523 MCM_gamma, averaged for days when NO was low, (< 0.1 ppb) and high (> 0.1 ppb). Net HO₂+NO₂ refers to
524 HO₂+NO₂→HO₂NO₂ minus HO₂NO₂→HO₂+NO₂.

525 Though there is not a strong dependence of HO₂ aerosol uptake loss pathway on NO mixing
526 ratio for the calculated γ_{HO_2} (av. 0.07 ± 0.035) within MCM_gamma, it can be seen that at the
527 lowest NO mixing ratios an average of ~7 % of total HO₂ loss is due to uptake, with a maximum
528 at the lowest NO of ~29% (shown as lilac dashed line in Figure 8). This is a significant loss of
529 HO₂, especially on days where the NO mixing ratio is low and the aerosol surface area is high,
530 highlighting that the uptake of HO₂ onto aerosols could be important, and will be increasingly
531 so at lower NO.

532 3.3.2 Comparison to γ_{HO_2} fixed at 0.2

533 While the maximum γ_{HO_2} calculated using the Song parameterisation for the summer AIRPRO
534 campaign was 0.15, to provide context with previous modelling studies, the commonly used
535 fixed value of $\gamma_{HO_2} = 0.2$ was added into the MCM_base model to give the MCM_SA model.
536 The average median diurnals of modelled OH, HO₂ and RO₂ (molecule cm⁻³) for MCM_base,
537 MCM_gamma and MCM_SA are shown in Figure 6.

538 In comparison to calculated γ_{HO_2} in MCM_gamma, a fixed $\gamma_{HO_2} = 0.2$ had a more significant
539 effect on radical concentrations. While the median diurnal shows that the RO₂ concentration
540 was not significantly affected by the addition of HO₂ uptake, the over-prediction seen in the
541 average median HO₂ concentration compared to the measurements at the 14:30 peak decreased



542 from a factor of ~ 2.9 in MCM_base to ~ 2.3 . OH radical concentrations were still relatively
543 well reproduced with early afternoon OH concentrations predicted better though this is due to
544 a shift in the modelled peak compared to the measured concentration peaking at midday.

545 As seen in Figure 9, the addition of $\gamma_{HO_2} = 0.2$ affected the ability of the model to reproduce
546 the NO dependence of radical concentrations. While MCM_base over-predicts HO_2 below ~ 1
547 ppb NO, the over-prediction of HO_2 decreases below 1 ppb NO for MCM_SA with HO_2 being
548 well reproduced at the lowest NO mixing ratios (i.e. < 0.1 ppb) due to the relative increase in
549 the importance of HO_2 uptake as a sink of HO_2 . Modelled RO_2 is not significantly affected by
550 the addition of HO_2 uptake at any NO mixing ratio. The modelled concentration of OH is under-
551 predicted for the entire range of NO mixing ratios compared to measured values, though only
552 slightly between ~ 1 and 6 ppb NO. Below ~ 4 ppb NO, the underprediction of OH by
553 MCM_SA increases compared to MCM_base due most likely to loss of HO_2 onto aerosols
554 competing with loss via NO to give OH. Budget analysis done by Whalley et al., 2021,
555 showcases that with a reduction in over-prediction of modelled HO_2 , OH is under-predicted
556 revealing a missing OH source.

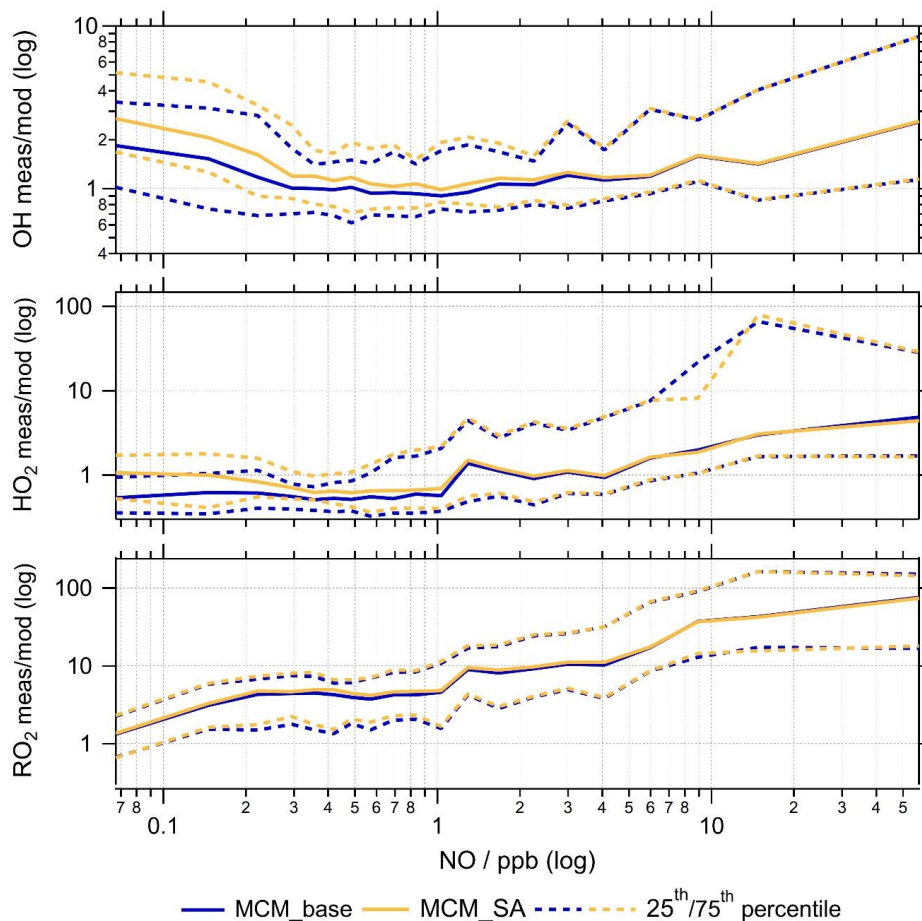


Figure 9. Ratio of measured to modelled OH, HO₂ and RO₂ radical concentrations using the MCM_base (blue) and MCM_SA (yellow) model binned over the range of NO mixing ratios (ppb) for the summer AIRPRO campaign. Solid lines show the median average measured to modelled radical concentration. Dashed lines show the 25th/75th percentile.

557 Analysis of the RODA for MCM_SA shows that with $\gamma_{HO_2} = 0.2$ HO₂ aerosol uptake is a
 558 significant contributor to total loss of HO₂ (8.1 ± 13 %, averaged for all NO mixing ratios).
 559 However, for all NO mixing ratios HO₂ + NO is still the dominant loss pathway (86 ± 18 %),
 560 as expected. At the lowest NO mixing ratios (i.e. < 0.1 ppb) an average of ~29 % of total HO₂
 561 loss is due to uptake, with a maximum at the lowest NO of ~78%, shown in Figure 10. The
 562 contribution of the various loss pathways of HO₂ to total HO₂ loss within MCM_gamma under
 563 low (< 0.1 ppb) and high (>0.1 ppb) NO are compared in Table 5. The comparison of



564 percentage contribution of HO₂ uptake to total HO₂ removal binned against NO mixing ratio
 565 (ppb) for MCM_gamma and MCM_SA RODA is shown in Figure 10.

	HO ₂ +O ₃	HO ₂ +OH	HO ₂ +HO ₂	HO ₂ +RO ₂	Net HO ₂ +NO ₂	HO ₂ +NO uptake
Low NO (< 0.1 ppb)	6.9 ± 3.5	0.1 ± 0.1	1.7 ± 1.4	17 ± 14	1.6 ± 2.2	44 ± 24
High NO (> 0.1 ppb)	1.8 ± 2.1	0.2 ± 0.2	0.6 ± 1.0	1.7 ± 3.8	0.4 ± 1.0	89 ± 13

566 **Table 5.** Average relative percentage contribution of individual HO₂ loss pathways to the total loss of HO₂ within
 567 MCM_SA (fixed $\gamma_{HO_2} = 0.2$), averaged for days when NO was low, (< 0.1 ppb) and high (> 0.1 ppb). Net
 568 HO₂+NO₂ refers to HO₂+NO₂→HO₂NO₂ minus HO₂NO₂→HO₂+NO₂.

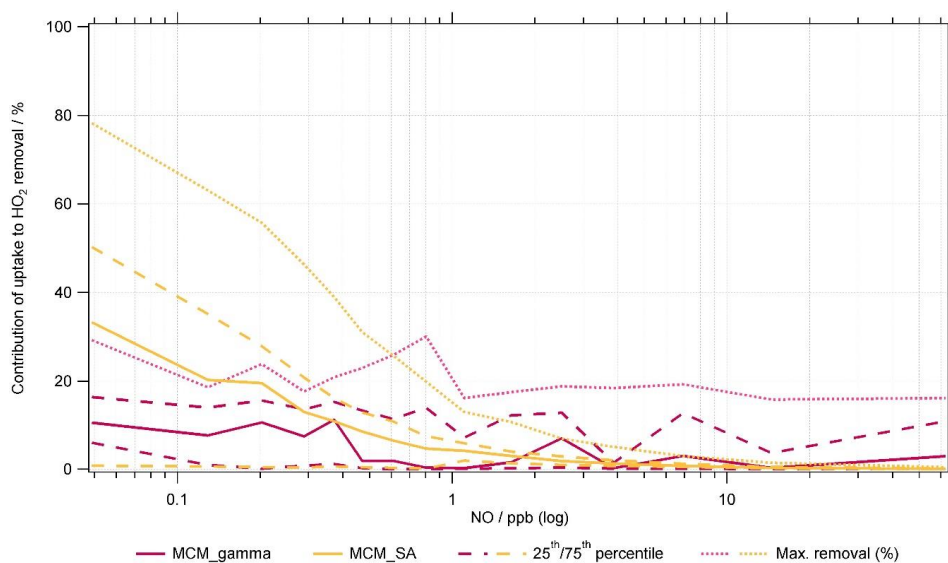


Figure 10. Average percentage contribution of HO₂ uptake to total HO₂ removal within MCM_gamma (pink line, $\gamma_{HO_2} = 0.070 \pm 0.035$) and MCM_SA model (yellow line, $\gamma_{HO_2} = 0.2$) for Summer AIRPRO campaign plotted as a function of NO mixing ratio (ppb). Dashed lines represent the 25th/75th percentiles. Dotted lines represent maximum removal.

569 3.3.3 Effect of γ_{HO_2} on the O₃ regime

570 3.3.3.1 Calculation of L_N/Q and absolute O₃ sensitivity

571 First introduced by Kleinman et al., 1997, L_N/Q is the ratio of radical loss via NO_x to total
 572 primary radical production and is used as a means of determining O₃ production sensitivity to
 573 VOCs and NO_x (Kleinman, 2000; Kleinman et al., 1997; Kleinman et al., 2001). This method
 574 was then built on by Sakamoto et al., 2019 who included loss of peroxy radicals
 575 (XO₂=HO₂+RO₂) onto aerosol surfaces within the calculation of O₃ sensitivity.



576 The only source of tropospheric O₃ is by the reaction of peroxy radicals with NO, while the
577 main source of XO₂ species is via the reaction of OH with VOCs.



578 The O₃ production rate in the troposphere is therefore:

$$P(O_3) = k_{HO_2+NO}[HO_2][NO] + k_{RO_2+NO}[RO_2][NO] \quad (2)$$

579 where k_{HO_2+NO} and k_{RO_2+NO} are the bimolecular rate constants for the reaction of HO₂ and
580 RO₂ with NO.

581 The production rate of OH, HO₂ and RO₂ radicals, Q, must equal the loss rate:

$$Q = L_P + L_N + L_R \quad (3)$$

582 where L_P is the loss rate of radicals onto aerosol particles, L_N is the loss rate of radicals via
583 reaction with NO_x species and L_R is the loss rate of radicals via radical-radical reactions to give
584 peroxides.

$$L_P = k_{HO_2 \text{ uptake}}[HO_2] + k_{RO_2 \text{ uptake}}[RO_2] = k_p[XO_2] \quad (4)$$

$$L_N \approx k_{NO_2+OH}[NO_2][OH] \quad (5)$$

$$L_R = 2(k_{HO_2+HO_2}[HO_2]^2 + k_{RO_2+HO_2}[HO_2][RO_2]) \quad (6)$$

585 where $k_{HO_2 \text{ uptake}}$ is the rate constant for the loss of HO₂ onto aerosol surfaces, $k_{RO_2 \text{ uptake}}$ is
586 the rate constant for the loss of RO₂ onto aerosol surfaces, k_{NO_2+OH} is the bimolecular rate
587 constant for the reaction of NO₂ with OH, $k_{HO_2+HO_2}$ is the bimolecular rate constant for the
588 self-reaction of HO₂ and $k_{RO_2+HO_2}$ is the bimolecular rate constant for the reaction of RO₂ with
589 HO₂.

590 For radical loss onto aerosol surfaces, the rate constant is given as a function of the reactive
591 uptake coefficient, γ_{XO_2} , aerosol particle surface area (cm² cm⁻³) and mean thermal velocity
592 (cm s⁻¹), given by $v = \sqrt{8RT/\pi M}$ with R, T and M as the gas constant, the absolute temperature
593 and the molar mass of species respectively.

$$k_{\text{radical uptake}} = \frac{\gamma_{XO_2} \times SA \times v}{4} \quad (7)$$

594 According to the method described in Sakamoto et al., 2019, the ratio of radical loss to NO_x to
595 primary O₃ production including radical loss via aerosol uptake, $\frac{L_N}{Q}$ is defined as follows:



$$\frac{L_N}{Q} = \frac{1}{1 + \left(\frac{(2k_R[XO_2] + k_P)k_{OH+VOC}[VOC]}{(1-\alpha)k_{HO_2+NO}[NO]k_{NO_2+OH}[NO_2]} \right)} \quad (8)$$

596 where k_{OH+VOC} is the bimolecular rate constant for the loss of OH via reaction with VOCs and
 597 $(1 - \alpha)$ is the fraction of XO_2 that is HO_2 .

598 The relative sensitivity of O_3 production to NO_x and VOCs is described by:

$$\frac{\delta \ln P(O_3)}{\delta \ln [NO_x]} = (1 - \chi) \left(\frac{1 - \frac{3}{2} \frac{L_N}{Q}}{1 - \frac{1}{2} \frac{L_N}{Q}} \right) + \chi \left(1 - 2 \frac{L_N}{Q} \right) \quad (9)$$

$$\frac{\delta \ln P(O_3)}{\delta \ln [VOC]} = (1 - \chi) \left(\frac{\frac{1}{2} \frac{L_N}{Q}}{1 - \frac{1}{2} \frac{L_N}{Q}} \right) + \chi \frac{L_N}{Q} \quad (10)$$

599 where $\chi = \frac{L_P}{L_P + L_R}$. The O_3 regime transition point, where $\frac{\delta \ln P(O_3)}{\delta \ln [NO_x]} = \frac{\delta \ln P(O_3)}{\delta \ln [VOC]}$, is given by $\frac{L_N}{Q_{trans}}$.

$$\frac{L_N}{Q_{trans}} = \frac{1}{2} (1 - \chi) + \frac{1}{3} \chi \quad (11)$$

600 Absolute O_3 sensitivity was introduced by Sakamoto et al., 2019, and allows for the assessment
 601 of how reduction in O_3 precursors could contribute to reduction in $P(O_3)$ by integrating over
 602 time and area. The absolute sensitivity of O_3 production to VOC and NO_x is then described by:

$$Absolute P(O_3) = \frac{\delta P(O_3)}{\delta \ln [X]} = P(O_3) \frac{\delta P(O_3)}{\delta \ln [X]} \quad (12)$$

603 where $[X]$ is NO_x or VOC.

604 $\frac{L_N}{Q}$ was calculated for all model runs, MCM_base, MCM_gamma and MCM_SA using
 605 modelled $[HO_2]$ and $[RO_2]$ concentrations but measured values of $[NO]$ and $[NO_2]$, to
 606 investigate the effect on the O_3 regime of adding HO_2 aerosol uptake into the model. The time
 607 series of calculated $\frac{L_N}{Q}$ for all models, in addition to the regime transition point, $\frac{L_N}{Q_{trans}}$ for the
 608 entire campaign is shown in Figure 11.

609 When $\frac{L_N}{Q} < \frac{L_N}{Q_{trans}}$, this is defined as a NO_x -sensitive regime, meaning that small changes in NO_x
 610 will affect the rate of in situ O_3 production. This can be seen on a few days across the campaign,
 611 specifically in the afternoon, due to NO_x peaking in the morning due to traffic emissions before
 612 rapidly decreasing in the afternoon which pushes the O_3 regime on certain days from VOC-



613 limited to NO_x -limited. However, for the majority of the campaign, the O_3 production regime
614 is VOC-limited, for all models, meaning that O_3 production rates will not be significantly
615 affected by small changes in NO_x .

616 Binning $\frac{L_N}{Q}$ against NO mixing ratio (ppb), in Figure 12, shows the change from VOC to NO_x -
617 limited regime at very low NO mixing ratios for MCM_base, MCM_gamma and MCM_SA.
618 As aerosol uptake is added the transition to NO_x -limited regime occurs at higher NO, with
619 average median transition point occurring at ~ 0.2 ppb NO for MCM_gamma (average $\gamma_{\text{HO}_2} =$
620 0.070 ± 0.035) and at ~ 0.5 ppb NO for MCM_SA (fixed $\gamma_{\text{HO}_2} = 0.2$). This suggests that a
621 reduction in PM (and therefore uptake of HO_2 onto aerosols) would delay the transition to a
622 NO_x -sensitive regime until lower NO_x levels are reached. Therefore, any emissions policy
623 aimed at reduced NO_x to decrease O_3 levels would not be as effective if PM is decreasing at
624 the same time.

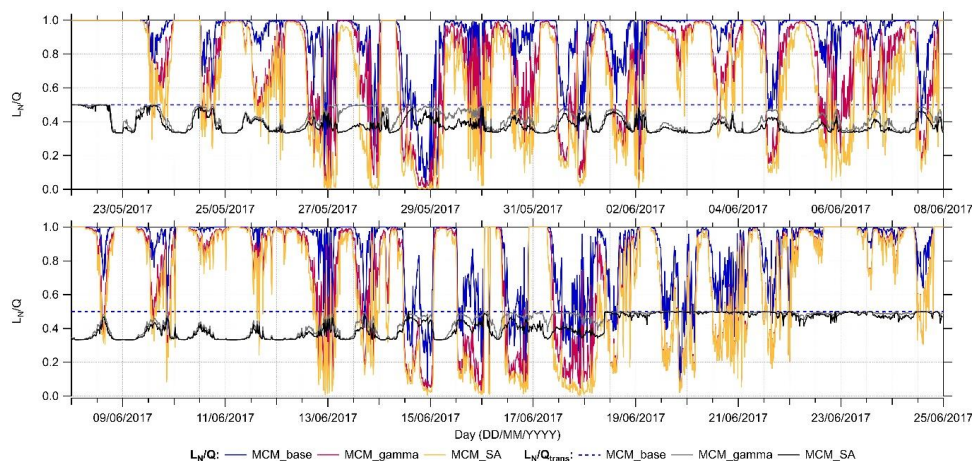


Figure 11. Time series of calculated $\frac{L_N}{Q}$ and $\frac{L_N}{Q_{trans}}$ values for MCM_base (blue), MCM_gamma (pink) and MCM_SA (yellow) models across the entire summer AIRPRO campaign. $\frac{L_N}{Q_{trans}}$ for MCM_gamma is shown as grey line, while $\frac{L_N}{Q_{trans}}$ for MCM_SA is the black line.

625

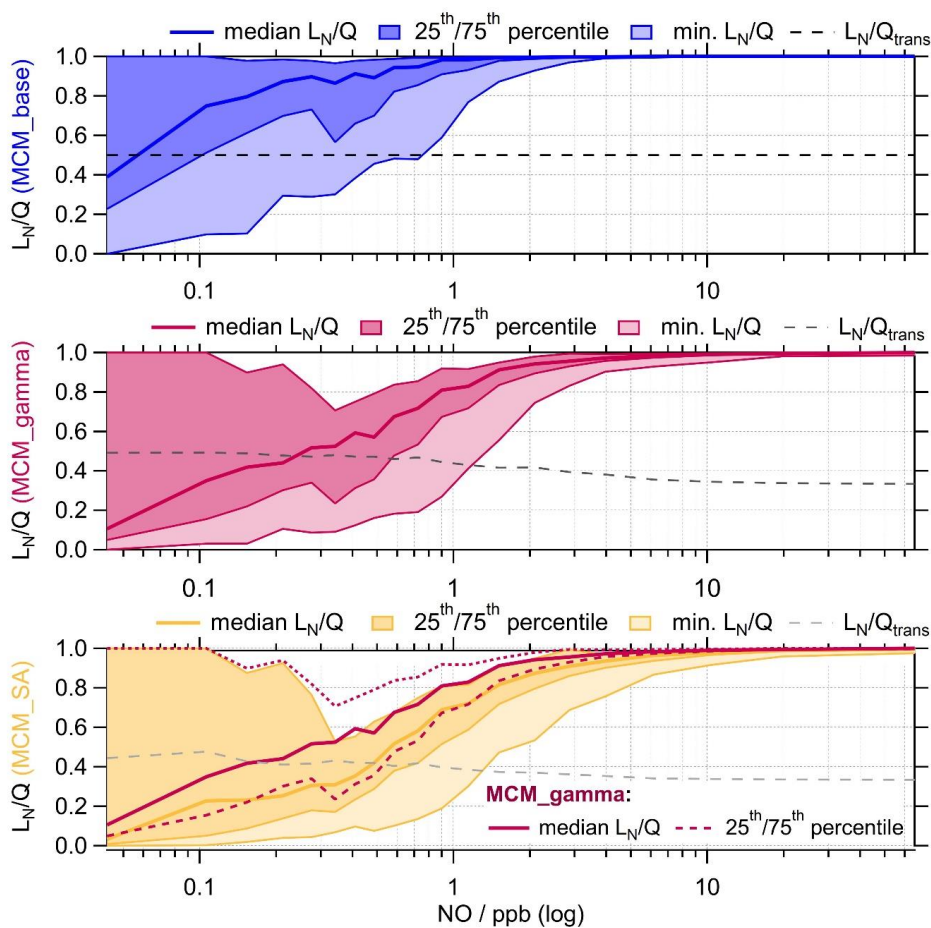


Figure 12. $\frac{L_N}{Q}$ for MCM_base (blue, top panel), MCM_gamma (pink, middle panel) and MCM_SA (yellow, bottom panel) binned against the log of measured NO mixing ratio for the entire summer AIRPRO campaign. $\frac{L_N}{Q_{trans}}$ for MCM_base (black dashed line) taken as 0.5 for entire range of NO mixing ratios. $\frac{L_N}{Q_{trans}}$ for MCM_gamma (dark grey dashed line) and MCM_SA (light grey dashed line) calculated using equation 11. 25th/75th percentiles and minimum $\frac{L_N}{Q}$ are plotted to show full spread of data for each model scenario.

626 The average median diurnal of absolute $P(O_3)$, $\frac{\delta P(O_3)}{\delta \ln [X]}$, for the MCM_gamma and MCM_SA
 627 over the entire campaign is shown in Figure 13. The time series of absolute $P(O_3)$, averaged up
 628 to a daily time resolution, across the entire measurement period can be found in Supplementary
 629 Information as SI Figure 2.

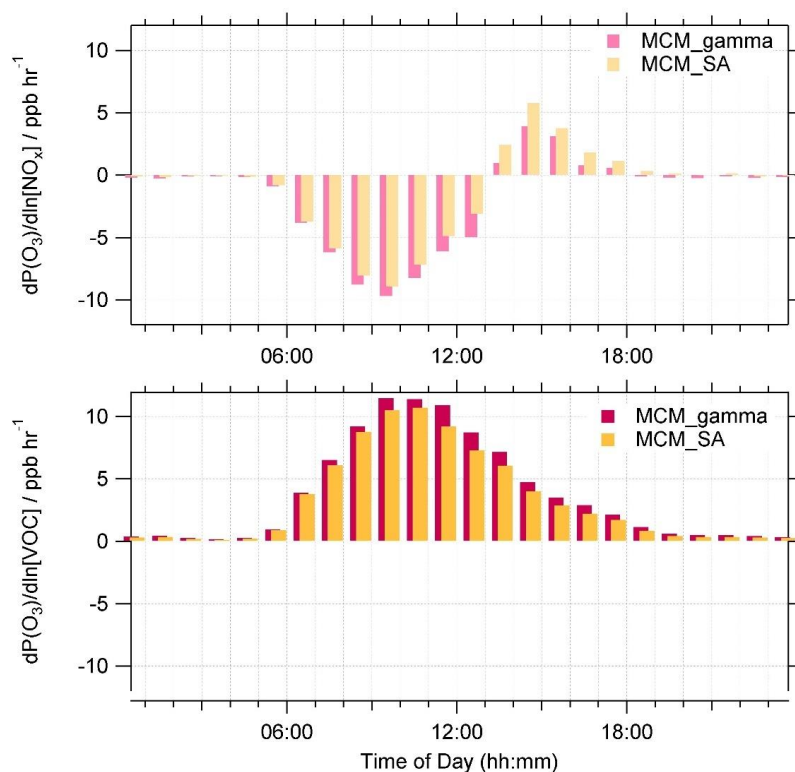


Figure 13. Average median diurnal of absolute O_3 sensitivity to NO_x (top panel) and VOC (bottom panel) in $ppbV h^{-1}$ for MCM_gamma (pink) and MCM_SA (yellow) across the entire summer AIRPRO campaign. MCM_gamma includes γ_{HO_2} calculated using the Song parameterisation (av. 0.070 ± 0.035) while MCM_SA includes γ_{HO_2} at a fixed value of 0.2. All diurnals are 60 minute averages.

630 As expected from $\frac{LN}{Q}$ calculations, calculations of absolute O_3 production sensitivity showcase
631 that for both MCM_gamma and MCM_SA, on average, the O_3 regime was VOC sensitive
632 throughout the day with NO_x sensitivity increasing in the afternoons. On a few days, when low
633 NO mixing ratio coincided with high SA, the O_3 regime can be seen shifting from VOC to NO_x
634 limited. An example of this can be found in SI Figure 3, for the 17/06/2017 and 18/06/2017
635 when the average NO mixing ratio was 0.41 ± 0.50 ppb and the average SA was $(8.4 \pm 6.2) \times$
636 $10^{-6} cm^2 cm^{-3}$. With an increase in γ_{HO_2} between MCM_gamma and MCM_SA, the sensitivity
637 of O_3 regime to VOC decreased but sensitivity to NO_x increased. This effect could be important
638 for areas where O_3 production regime is NO_x sensitive or less strongly VOC sensitive. With
639 NO_x levels reportedly decreasing across China in recent years (Krotkov et al., 2016; Liu et al.,
640 2016; Miyazaki et al., 2017; Van Der A et al., 2017), O_3 production regimes would be expected
641 to move more towards NO_x -sensitive regimes in urban China. However, with concomitant



642 reduction in PM (Ma et al., 2016b; Lin et al., 2018), this transition to a NO_x -sensitive regime
643 may be delayed until lower NO_x levels are reached.

644 Our result for the Beijing campaign are consistent with the results of Song et al., 2022 which
645 concluded that for the conditions of the Wangdu campaign the addition of HO_2 uptake does not
646 change the overall O_3 sensitivity regime throughout the campaign. However, the shift in O_3
647 sensitivity regime from VOC-limited to NO_x -limited from the consideration of HO_2 uptake
648 could be important for areas with lower NO_x and high aerosol particle loading.

649 **4 Conclusions**

650 Using the Song parameterisation, the heterogeneous uptake coefficient of HO_2 , γ_{HO_2} , was
651 calculated for the summer AIRPRO campaign in Beijing, 2017 as a function of measured
652 $[\text{Cu}^{2+}]_{\text{eff}}$, $[\text{ALWC}]$ and $[\text{PM}]$. The calculated average $\gamma_{\text{HO}_2} = 0.070 \pm 0.035$ (ranging from 0.002
653 to 0.15 across the campaign) was significantly lower than the fixed value of $\gamma_{\text{HO}_2} = 0.2$
654 commonly used in modelling studies. This calculated value was similar, however, to values
655 calculated for the Wangdu 2014 summer campaign in China (Tan et al., 2020; Song et al.,
656 2020). Using the calculated γ_{HO_2} , the OH, HO_2 and RO_2 radical concentrations were modelled
657 using the Master Chemical Mechanism, and compared to the measured campaign values, with
658 and without the addition of HO_2 aerosol uptake. Due to the low calculated value of γ_{HO_2} , and
659 the high levels of NO, rate of destruction analysis showed the dominant HO_2 loss pathway to
660 be $\text{HO}_2 + \text{NO}$ for all NO mixing ratios with HO_2 uptake not contributing significantly to the
661 loss of HO_2 ($< 2\%$). However, at the lowest NO mixing ratios (i.e. < 0.1 ppb) HO_2 loss onto
662 aerosols contributed up to a maximum of 29 % of the total HO_2 loss. Using the modelled HO_2
663 and RO_2 radical concentrations for model scenarios with and without HO_2 uptake, showed that
664 on average the O_3 production regime was VOC-limited across the entire campaign with the
665 exception of several days with low NO mixing ratio where the regime tended towards NO_x -
666 limited, meaning that small changes in NO_x would not have a large effect on the O_3 production
667 for this summer period in Beijing, however changes in HO_2 uptake could. While the addition
668 of the calculated uptake coefficient did not change the overall O_3 regime across the campaign,
669 with the O_3 production regime remaining strongly VOC-limited, the transition from a VOC-
670 sensitive to NO_x -sensitive O_3 regime occurs at higher NO_x . This means that for Beijing, where
671 the O_3 production regime is strongly VOC-sensitive and NO_x levels are high, any policy
672 looking to reduce O_3 via the reduction of NO_x needs to consider concurrent PM reduction
673 policies which may affect HO_2 uptake. In cleaner environments, where NO_x levels are lower,



674 but aerosol surface area is still high, lower values of γ_{HO_2} , i.e. less than 0.2, could have a more
675 significant effect on both overall HO₂ concentration and the O₃ production regime.

676 *Data availability.* Data presented in this study can be obtained from authors upon request
677 (d.e.heard@leeds.ac.uk)

678 *Author contributions.* LKW, EJS, RWM, CY and DEH carried out the radical measurements.
679 LKW and EJS developed the model and JED performed the calculations. JDL, FS, JRH, RED,
680 MS, JFH, ACL, AM, SDW, AB, TJB, HC, BO, CJP, CNH, RLJ, LRC, LJK, WJFA, WJB, SS,
681 JX, TV, ZS, RMH, SK, SG, YS, WX, SY, LW, PF and XW provided logistical support and
682 supporting data to constrain the model. JED prepared the manuscript with contributions from
683 all co-authors.

684 *Competing interests.* The authors declare that they have no conflict of interest.

685 *Acknowledgements.* We are grateful to the Natural Environmental Research Council for
686 funding a SPHERES PhD studentship (Joanna E. Dyson). We are grateful to Tuan Vu for
687 providing supervision and supporting data.

688 5 References

689 Bohn, B., Heard, D. E., Mihalopoulos, N., Plass-Dülmer, C., Schmitt, R., and Whalley, L. K.:
690 Characterisation and improvement of j(O¹D) filter radiometers, *Atmos. Meas. Tech.*, 9, 3455-
691 3466, <https://doi.org/10.5194/amt-9-3455-2016>, 2016.

692 Brauer, M., Freedman, G., Frostad, J., van Donkelaar, A., Martin, R. V., Dentener, F.,
693 Dingenen, R. v., Estep, K., Amini, H., Apte, J. S., Balakrishnan, K., Barregard, L., Broday,
694 D., Feigin, V., Ghosh, S., Hopke, P. K., Knibbs, L. D., Kokubo, Y., Liu, Y., Ma, S.,
695 Morawska, L., Sangrador, J. L. T., Shaddick, G., Anderson, H. R., Vos, T., Forouzanfar, M.
696 H., Burnett, R. T., and Cohen, A.: Ambient Air Pollution Exposure Estimation for the Global
697 Burden of Disease 2013, *Environ. Sci. Technol.*, 50, 79-88,
698 <https://doi.org/10.1021/acs.est.5b03709>, 2016.

699 Commane, R., Floquet, C. F. A., Ingham, T., Stone, D., Evan, M. J., and Heard, D. E.:
700 Observations of OH and HO₂ radicals over West Africa, *Atmos. Chem. Phys.*, 10, 8783-8801,
701 <https://doi.org/10.5194/acp-10-8783-2010>, 2010.

702 Cooper, P. L. and Abbatt, J. P. D.: Heterogeneous Interactions of OH and HO₂ Radicals with
703 Surfaces Characteristic of Atmospheric Particulate Matter, *The Journal of Physical*
704 *Chemistry*, 100, 2249-2254, <https://doi.org/10.1021/jp952142z>, 1996.



- 705 Crilley, L. R., Kramer, L., Pope, F. D., Whalley, L. K., Cryer, D. R., Heard, D. E., Lee, J. D.,
706 Reed, C., and Bloss, W. J.: On the interpretation of in situ HONO observations via
707 photochemical steady state, *Faraday Discuss.*, 189, 191-212,
708 <https://doi.org/10.1039/c5fd00224a>, 2016.
- 709 Dunmore, R., Hopkins, J., Lidster, R., Lee, J., Evans, M., Rickard, A., Lewis, A., and
710 Hamilton, J.: Diesel-related hydrocarbons can dominate gas phase reactive carbon in
711 megacities, *Atmos. Chem. Phys.*, 15, 9983-9996, <https://doi.org/10.5194/acp-15-9983-2015>,
712 2015.
- 713 Forster, P., Ramaswamy, V., Artaxo, P., Berntsen, T., Betts, R., Fahey, D. W., Haywood, J.,
714 Lean, J., Lowe, D. C., Myhre, G., Nganga, J., Prinn, R., Raga, G., Schulz, M., and Dorland,
715 R. V.: Chapter 2. Changes in atmospheric constituents and in radiative forcing. , *Climate
716 Change 2007. The Physical Science Basis*, 2007.
- 717 Fountoukis, C. and Nenes, A.: ISORROPIA II: a computationally efficient thermodynamic
718 equilibrium model for K^+ - Ca^{2+} - Mg^{2+} - NH_4^+ - Na^+ - SO_4^{2-} - NO_3^- - Cl^- - H_2O aerosols, *Atmos. Chem.
719 Phys.*, 7, 4639-4659, <https://doi.org/10.5194/acp-7-4639-2007>, 2007.
- 720 Fuchs, H., Holland, F., and Hofzumahaus, A.: Measurement of tropospheric RO_2 and HO_2
721 radicals by a laser-induced fluorescence instrument, *The Review of scientific instruments*, 79,
722 084104, <https://doi.org/10.1063/1.2968712>, 2008.
- 723 Gakidou, E., Afshin, A., Abajobir, A. A., Abate, K. H., Abbafati, C., Abbas, K. M., Abd-
724 Allah, F., Abdulle, A. M., Abera, S. F., and Aboyans, V.: Global, regional, and national
725 comparative risk assessment of 84 behavioural, environmental and occupational, and
726 metabolic risks or clusters of risks, 1990–2016: a systematic analysis for the Global Burden
727 of Disease Study 2016, *The Lancet*, 390, 1345-1422, [https://doi.org/10.1016/S0140-
728 6736\(18\)32279-7](https://doi.org/10.1016/S0140-6736(18)32279-7), 2017.
- 729 George, I. J., Matthews, P. S. J., Whalley, L. K., Brooks, B., Goddard, A., Baeza-Romero,
730 M., and Heard, D. E.: Measurements of uptake coefficients for heterogeneous loss of HO_2
731 onto submicron inorganic salt aerosols., *Phys. Chem. Chem. Phys.*, 15, 12829-12845,
732 <https://doi.org/10.1039/c3cp51831k>, 2013.
- 733 Hopkins, J. R., Jones, C. E., and Lewis, A. C.: A dual channel gas chromatograph for
734 atmospheric analysis of volatile organic compounds including oxygenated and monoterpene
735 compounds., *J. Environ. Monit.*, 13, 2268-2276, <https://doi.org/10.1039/C1EM10050E>, 2011.
- 736 Ivatt, P. D., Evans, M. J., and Lewis, A. C.: Suppression of surface ozone by an aerosol-
737 inhibited photochemical ozone regime, *Nat. Geosci.*, 15, 536-540,
738 <https://doi.org/10.1038/s41561-022-00972-9>, 2022.



- 739 Jacob, D. J.: Heterogeneous chemistry and tropospheric ozone, *Atmos. Environ.*, 34, 2131-
740 2159, [https://doi.org/10.1016/S1352-2310\(99\)00462-8](https://doi.org/10.1016/S1352-2310(99)00462-8), 2000.
- 741 Jin, Y., Andersson, H., and Zhang, S.: Air Pollution Control Policies in China: A
742 Retrospective and Prospects, *Int. J. Environ. Res. Public Health*, 13,
743 <https://doi.org/10.3390/ijerph13121219>, 2016.
- 744 Kanaya, Y. G., Cao, R. Q., Kato, S. G., Miyakawa, Y. K., Kajii, Y., Tanimoto, H., Yokouchi,
745 Y., Mochida, M., Kawamura, K., and Akimoto, H.: Chemistry of OH and HO₂ radicals
746 observed at Rishiri Island, Japan, in September 2003: Missing daytime sink of HO₂ and
747 positive nighttime correlations with monoterpenes, *J. Geophys. Res. Atmos.*, 112, D11308,
748 <https://doi.org/10.1029/2006JD007987>, 2007.
- 749 Kleinman, L. I.: Ozone process insights from field experiments – part II: Observation-based
750 analysis for ozone production, *Atmos. Environ.*, 34, 2023-2033,
751 [https://doi.org/10.1016/S1352-2310\(99\)00457-4](https://doi.org/10.1016/S1352-2310(99)00457-4), 2000.
- 752 Kleinman, L. I., Daum, P. H., Lee, Y.-N., Nunnermacker, L. J., Springston, S. R., Weinstein-
753 Lloyd, J., and Rudolph, J.: Sensitivity of ozone production rate to ozone precursors, *Geophys.*
754 *Res. Lett.*, 28, 2903-2906, <https://doi.org/10.1029/2000GL012597>, 2001.
- 755 Kleinman, L. I., Daum, P. H., Lee, J. H., Lee, Y.-N., Nunnermacker, L. J., Springston, S. R.,
756 Newman, L., Weinstein-Lloyd, J., and Sillman, S.: Dependence of ozone production on NO
757 and hydrocarbons in the troposphere, *Geophys. Res. Lett.*, 24, 2299-2302,
758 <https://doi.org/10.1029/97GL02279>, 1997.
- 759 Krotkov, N. A., McLinden, C. A., Li, C., Lamsal, L. N., Celarier, E. A., Marchenko, S. V.,
760 Swartz, W. H., Bucsela, E. J., Joiner, J., Duncan, B. N., Boersma, K. F., Veefkind, J. P.,
761 Levelt, P. F., Fioletov, V. E., Dickerson, R. R., He, H., Lu, Z., and Streets, D. G.: Aura OMI
762 observations of regional SO₂ and NO₂ pollution changes from 2005 to 2015, *Atmos. Chem.*
763 *Phys.*, 16, 4605-4629, <https://doi.org/10.5194/acp-16-4605-2016>, 2016.
- 764 Lakey, P. S. J., George, I. J., Baeza-Romero, M., Whalley, L. K., and Heard, D. E.: Organics
765 substantially reduce HO₂ uptake onto aerosols containing transition metal ions. , *J. Phys.*
766 *Chem. A*, 120, 1421-1430, <https://doi.org/10.1021/acs.jpca.5b06316>, 2016.
- 767 Lakey, P. S. J., George, I. J., Whalley, L. K., Baeza-Romero, M., and Heard, D. E.:
768 Measurements of HO₂ uptake coefficients onto single component organic aerosols.,
769 *Environmental Science Technology*, 49, 4878-4885, <https://doi.org/10.1021/acs.est.5b00948>,
770 2015.
- 771 Le Breton, M., Bacak, A., Muller, J. B. A., Bannan, T. J., Kennedy, O., Ouyang, B., Xiao, P.,
772 Bauguitte, S. J. B., Shallcross, D. E., Jones, R. L., Daniels, M. J. S., Ball, S. M., and Percival,



- 773 C. J.: The first airborne comparison of N₂O₅ measurements over the UK using a CIMS and
774 BBCEAS during the RONOCO campaign, *Analytical Methods*, 6, 9731-9743,
775 <https://doi.org/10.1039/C4AY02273D>, 2014.
- 776 Levy, H.: Normal atmosphere: large radical and formaldehyde concentrations predicted,
777 *Science*, 173, 141-143, <https://doi.org/10.1126/science.173.3992.141>, 1971.
- 778 Li, H., Wang, D., Cui, L., Gao, Y., Huo, J., Wang, X., Zhang, Z., Tan, Y., Huang, Y., and
779 Cao, J. J. S. o. t. t. e.: Characteristics of atmospheric PM_{2.5} composition during the
780 implementation of stringent pollution control measures in shanghai for the 2016 G20 summit,
781 648, 1121-1129, <https://doi.org/10.1016/j.scitotenv.2018.08.219>, 2019.
- 782 Li, K., Jacob, D. J., Liao, H., Shen, L., Zhang, Q., and Bates, K.: Anthropogenic drivers of
783 2013-2017 trends in summer surface ozone in China, *Proceedings of the National Academy*
784 *of Sciences*, 116, 422-427, <https://doi.org/10.1073/pnas.1812168116>, 2018.
- 785 Lin, C. Q., Liu, G., Lau, A. K. H., Li, Y., Li, C. C., Fung, J. C. H., and Lao, X. Q.: High-
786 resolution satellite remote sensing of provincial PM_{2.5} trends in China from 2001 to 2015,
787 *Atmos. Environ.*, 180, 110-116, <https://doi.org/10.1016/j.atmosenv.2018.02.045>, 2018.
- 788 Liu, F., Zhang, Q., van der A, R. J., Zheng, B., Tong, D., Yan, L., Zheng, Y., and He, K.:
789 Recent reduction in NO_x emissions over China: synthesis of satellite observations and
790 emission inventories, *Environ. Res. Lett.*, 11, 114002, <https://doi.org/10.1088/1748-9326/11/11/114002>, 2016.
- 791 [9326/11/11/114002](https://doi.org/10.1088/1748-9326/11/11/114002), 2016.
- 792 Liu, Y.-H., Liao, W.-Y., Lin, X.-F., Li, L., and Zeng, X.-l.: Assessment of Co-benefits of
793 vehicle emission reduction measures for 2015–2020 in the Pearl River Delta region, China,
794 *Environ. Pollut.*, 223, 62-72, <https://doi.org/10.1016/j.envpol.2016.12.031>, 2017.
- 795 Ma, Z., Xu, J., Quan, W., Zhang, Z., Lin, W., and Xu, X.: Significant increase of surface
796 ozone at a rural site, north of eastern China, *Atmos. Chem. Phys.*, 16, 3969-3977,
797 <https://doi.org/10.5194/acp-16-3969-2016>, 2016a.
- 798 Ma, Z., Hu, X., Sayer, A. M., Levy, R., Zhang, Q., Xue, Y., Tong, S., Bi, J., Huang, L., and
799 Liu, Y.: Satellite-Based Spatiotemporal Trends in PM_{2.5} Concentrations: China, 2004-2013,
800 *Environ. Health Perspect.*, 124, 184-192, <https://doi.org/10.1289/ehp.1409481>, 2016b.
- 801 Mao, J., Fan, S., Jacob, D. J., and Travis, K. R.: Radical loss in the atmosphere from Cu-Fe
802 redox coupling in aerosols, *Atmos. Chem. Phys.*, 13, 509-519, <https://doi.org/10.5194/acp-13-509-2013>, 2013.
- 803 [13-509-2013](https://doi.org/10.5194/acp-13-509-2013), 2013.
- 804 Mao, J., Jacob, D. J., Evans, M. J., Olson, J. R., Ren, X., Brune, W. H., Chair, J. M. S.,
805 Crouse, J. D., Spencer, K. M., Beaver, M. R., Wennberg, P. O., Cubison, M. J., Jimenez, J.
806 L., Fried, A., Weibring, P., Walega, J. G., Hall, S. R., Weinheimer, A. J., Cohen, R. C., Chen,



- 807 G., Crawford, J. H., McHaughton, C., Clarke, A. D., Jaegle, L., Fisher, J. K., Yantosca, R.
808 M., LeSager, P., and Carouge, C.: Chemistry of hydrogen oxide radicals (HO_x) in the arctic
809 troposphere in spring, *Atmos. Chem. Phys.*, 10, 5823-5838, [https://doi.org/10.5194/acp-10-](https://doi.org/10.5194/acp-10-5823-2010)
810 [5823-2010](https://doi.org/10.5194/acp-10-5823-2010), 2010.
- 811 Martinez, M., Harder, H., Kovacs, T. A., Simpas, J. B., Bassis, J., Leshner, R., Brune, W. H.,
812 Frost, G. J., Williams, E. J., Stroud, C. A., Jobson, B. T., Roberts, J. M., Hall, S. R., Shetter,
813 R. E., Wert, B., Fried, A., Alicke, B., Stutz, J., Young, V. L., White, A. B., and Zamora, R. J.:
814 OH and HO_2 concentrations, sources, and loss rates during the Southern Oxidants Study in
815 Nashville, Tennessee, summer 1999, *Journal of Geophysical Research: Atmospheres*, 108,
816 <https://doi.org/10.1029/2003JD003551>, 2003.
- 817 Matthews, P. S. J., Baeza-Romero, M., Whalley, L. K., and Heard, D. E.: Uptake of HO_2
818 radicals onto Arizona test dust particles using an aerosol flow tube, *Atmos. Chem. Phys.*, 14,
819 7397-7408, <https://doi.org/10.5194/acp-14-7397-2014>, 2014.
- 820 Miyazaki, K., Eskes, H., Sudo, K., Boersma, K. F., Bowman, K., and Kanaya, Y.: Decadal
821 changes in global surface NO_x emissions from multi-constituent satellite data assimilation,
822 *Atmos. Chem. Phys.*, 17, 807-837, <https://doi.org/10.5194/acp-17-807-2017>, 2017.
- 823 Mozurkewich, M., McMurry, P. H., Gupta, A., and Calvert, J. G.: Mass accommodation
824 coefficient for HO_2 radicals on aqueous particles, *J. Geophys. Res.*, 92, 4163-4170,
825 <https://doi.org/10.1029/JD092iD04p04163>, 1987.
- 826 Sakamoto, Y., Sadanaga, Y., Li, J., Matsuoka, K., Takemura, M., Fujii, T., Nakagawa, M.,
827 Kohno, N., Nakashima, Y., Sato, K., Nakayama, T., Kato, S., Takami, A., Yoshino, A.,
828 Murano, K., and Kajii, Y.: Relative and Absolute Sensitivity Analysis on Ozone Production
829 in Tsukuba, a City in Japan, *Environ. Sci. Technol.*, 53, 13629-13635,
830 <https://doi.org/10.1021/acs.est.9b03542>, 2019.
- 831 Shi, Z., Vu, T., Kotthaus, S., Harrison, R. M., Grimmond, S., Yue, S., Zhu, T., Lee, J., Han,
832 Y., Demuzere, M., Dunmore, R. E., Ren, L., Liu, D., Wang, Y., Wild, O., Allan, J., Acton,
833 W. J., Barlow, J., Barratt, B., Beddows, D., Bloss, W. J., Calzolari, G., Carruthers, D.,
834 Carslaw, D. C., Chan, Q., Chatzidiakou, L., Chen, Y., Crilley, L., Coe, H., Dai, T., Doherty,
835 R., Duan, F., Fu, P., Ge, B., Ge, M., Guan, D., Hamilton, J. F., He, K., Heal, M., Heard, D.,
836 Hewitt, C. N., Hollaway, M., Hu, M., Ji, D., Jiang, X., Jones, R., Kalberer, M., Kelly, F. J.,
837 Kramer, L., Langford, B., Lin, C., Lewis, A. C., Li, J., Li, W., Liu, H., Liu, J., Loh, M., Lu,
838 K., Lucarelli, F., Mann, G., McFiggans, G., Miller, M. R., Mills, G., Monk, P., Nemitz, E.,
839 O'Connor, F., Ouyang, B., Palmer, P. I., Percival, C., Popoola, O., Reeves, C., Rickard, A. R.,
840 Shao, L., Shi, G., Spracklen, D., Stevenson, D., Sun, Y., Sun, Z., Tao, S., Tong, S., Wang, Q.,



- 841 Wang, W., Wang, X., Wang, X., Wang, Z., Wei, L., Whalley, L., Wu, X., Wu, Z., Xie, P.,
842 Yang, F., Zhang, Q., Zhang, Y., Zhang, Y., and Zheng, M.: Introduction to the special issue
843 “In-depth study of air pollution sources and processes within Beijing and its surrounding
844 region (APHH-Beijing)”, *Atmos. Chem. Phys.*, 19, 7519-7546, [https://doi.org/10.5194/acp-](https://doi.org/10.5194/acp-19-7519-2019)
845 [19-7519-2019](https://doi.org/10.5194/acp-19-7519-2019), 2019.
- 846 Silver, B., Reddington, C. L., Arnold, S. R., and Spracklen, D. V.: Substantial changes in air
847 pollution across China during 2015–2017, *Environ. Res. Lett.*, 13, 114012,
848 <https://doi.org/10.1088/1748-9326/aae718>, 2018.
- 849 Slater, E. J.: Understanding radical chemistry in Beijing through observations and modelling,
850 School of Chemistry, University of Leeds, 2020.
- 851 Slater, E. J., Whalley, L. K., Woodward-Massey, R., Ye, C., Lee, J. D., Squires, F., Hopkins,
852 J. R., Dunmore, R. E., Shaw, M., Hamilton, J. F., Lewis, A. C., Crilley, L. R., Kramer, L.,
853 Bloss, W., Vu, T., Sun, Y., Xu, W., Yue, S., Ren, L., Acton, W. J. F., Hewitt, C. N., Wang,
854 X., Fu, P., and Heard, D. E.: Elevated levels of OH observed in haze events during
855 wintertime in central Beijing, *Atmos. Chem. Phys. Discuss.*, 2020, 1-43,
856 <https://doi.org/10.5194/acp-2020-362>, 2020.
- 857 Smith, K. R., Edwards, P. M., Evans, M. J., Lee, J. D., Shaw, M. D., Squires, F., Wilde, S.,
858 and Lewis, A. C.: Clustering approaches to improve the performance of low cost air pollution
859 sensors, *Faraday Discuss.*, 200, 621-637, <https://doi.org/10.1039/C7FD00020K>, 2017.
- 860 Sommariva, R., Haggerstone, A. L., Carpenter, L. J., Carslaw, N., Creasey, D. J., Heard, D.
861 E., Lee, J. D., Lewis, A. C., Pilling, M. J., and Zador, J.: OH and HO₂ chemistry in clean
862 marine air during SOAPEX-2, *Atmos. Chem. Phys.*, 4, 839-856, [https://doi.org/10.5194/acp-](https://doi.org/10.5194/acp-4-839-2004)
863 [4-839-2004](https://doi.org/10.5194/acp-4-839-2004), 2004.
- 864 Song, H., Lu, K., Dong, H., Tan, Z., Chen, S., Zeng, L., and Zhang, Y.: Reduced Aerosol
865 Uptake of Hydroperoxyl Radical May Increase the Sensitivity of Ozone Production to
866 Volatile Organic Compounds, *Environ. Sci. Tech. Letts.*, 9, 22-29,
867 <https://doi.org/10.1021/acs.estlett.1c00893>, 2022.
- 868 Song, H., Chen, X., Lu, K., Zou, Q., Tan, Z., Fuchs, H., Wiedensohler, A., Moon, D. R.,
869 Heard, D. E., Baeza-Romero, M. T., Zheng, M., Wahner, A., Kiendler-Scharr, A., and Zhang,
870 Y.: Influence of aerosol copper on HO₂ uptake: a novel parameterized equation, *Atmos.*
871 *Chem. Phys.*, 20, 15835-15850, <https://doi.org/10.5194/acp-20-15835-2020>, 2020.
- 872 Stone, D., Whalley, L. K., Ingham, T., Edwards, P. M., Cryer, D. R., Brumby, C. A., Seakins,
873 P. W., and Heard, D. E.: Measurement of OH reactivity by laser flash photolysis coupled



874 with laser-induced fluorescence spectroscopy, *Atmos. Meas. Tech.*, 9, 2827-2844,
875 <https://doi.org/10.5194/amt-9-2827-2016>, 2016.

876 Taketani, F., Kanaya, Y., and Akimoto, H.: Kinetics of heterogeneous reactions of HO₂
877 radical at ambient concentration levels with (NH₄)₂SO₄ and NaCl aerosol particles., *J. Phys.*
878 *Chem. A*, 112, 2370-2377, <https://doi.org/10.1021/jp0769936>, 2008.

879 Taketani, F., Kanaya, Y., Pocharnart, P., Liu, Y., Li, J., Okuzawa, K., Kawamura, K., Wang,
880 Z., and Akimoto, H.: Measurement of overall uptake coefficients for HO₂ radicals by aerosol
881 particles sampled from ambient air at Mts. Tai and Mang (China). *Atmos. Chem. Phys.*, 12,
882 11907-11916, <https://doi.org/10.5194/acp-12-11907-2012>, 2012.

883 Tan, Z., Hofzumahaus, A., Lu, K., Brown, S. S., Holland, F., Huey, L. G., Kiendler-Scharr,
884 A., Li, X., Liu, X., Ma, N., Min, K.-E., Rohrer, F., Shao, M., Wahner, A., Wang, Y.,
885 Wiedensohler, A., Wu, Y., Wu, Z., Zeng, L., Zhang, Y., and Fuchs, H.: No Evidence for a
886 Significant Impact of Heterogeneous Chemistry on Radical Concentrations in the North
887 China Plain in Summer 2014, *Environ. Sci. Technol.*, 54, 5973-5979,
888 <https://doi.org/10.1021/acs.est.0c00525>, 2020.

889 Thornton, J. A. and Abbatt, J. P. D.: Measurements of HO₂ uptake of aqueous aerosol: Mass
890 accommodation coefficients and net reactive loss., *J. Geophys. Res.*, 110,
891 <https://doi.org/10.1029/2004JD005402>, 2005.

892 Thornton, J. A., Jaegle, L., and McNeill, V. F.: Assessing known pathways for HO₂ loss in
893 aqueous atmospheric aerosols: Regional and global impacts on tropospheric oxidants. , *J.*
894 *Geophys. Res.*, 113, <https://doi.org/10.1029/2007JD009236>, 2008.

895 van der A, R. J., Mijling, B., Ding, J., Koukouli, M. E., Liu, F., Li, Q., Mao, H., and Theys,
896 N.: Cleaning up the air: effectiveness of air quality policy for SO₂ and NO_x emissions in
897 China, *Atmos. Chem. Phys.*, 17, 1775-1789, <https://doi.org/10.5194/acp-17-1775-2017>, 2017.

898 Verstraeten, W. W., Neu, J. L., Williams, J. E., Bowman, K. W., Worden, J. R., and
899 Boersma, K. F.: Rapid increases in tropospheric ozone production and export from China,
900 *Nat. Geosci.*, 8, 690-695, <https://doi.org/10.1038/ngeo2493>, 2015.

901 Wang, P.: China's air pollution policies: Progress and challenges, *Current Opinion in*
902 *Environmental Science & Health*, 19, 100227, <https://doi.org/10.1016/j.coesh.2020.100227>,
903 2021.

904 Whalley, L. K., Blitz, M. A., Desservattez, M., Seakins, P. W., and Heard, D. E.: Reporting
905 the sensitivity of laser-induced fluorescence instruments used for HO₂ detection to an
906 interference from RO₂ radicals and introducing a novel approach that enables HO₂ and



907 certain RO₂ types to be selectively measured, *Atmos. Meas. Tech.*, 6, 3425-3440,
908 <https://doi.org/10.5194/amt-6-3425-2013>, 2013.

909 Whalley, L. K., Stone, D., Bandy, B., Dunmore, R., Hamilton, J. F., Hopkins, J., Lee, J. D.,
910 Lewis, A. C., and Heard, D. E.: Atmospheric OH reactivity in central London: observations,
911 model predictions and estimates of in situ ozone production, *Atmos. Chem. Phys.*, 16, 2109-
912 2122, <https://doi.org/10.5194/acp-16-2109-2016>, 2016.

913 Whalley, L. K., Stone, D., Dunmore, R., Hamilton, J., Hopkins, J. R., Lee, J. D., Lewis, A.
914 C., Williams, P., Kleffmann, J., Laufs, S., Woodward-Massey, R., and Heard, D. E.:
915 Understanding in situ ozone production in the summertime through radical observations and
916 modelling studies during the Clean air for London project (ClearfLo), *Atmos. Chem. Phys.*,
917 18, 2547-2571, <https://doi.org/10.5194/acp-18-2547-2018>, 2018.

918 Whalley, L. K., Furneaux, K. L., Goddard, A., Lee, J. D., Mahajan, A., Oetjen, H., Read, K.
919 A., Kaaden, N., Carpenter, L. J., Lewis, A. C., Plane, J. M. C., Saltzman, E. S.,
920 Wiedensohler, A., and Heard, D. E.: The chemistry of OH and HO₂ radicals in the boundary
921 layer over the tropical Atlantic Ocean, *Atmos. Chem. Phys.*, 10, 1555-1576,
922 <https://doi.org/10.5194/acp-10-1555-2010>, 2010.

923 Whalley, L. K., Slater, E. J., Woodward-Massey, R., Ye, C., Lee, J. D., Squires, F., Hopkins,
924 J. R., Dunmore, R. E., Shaw, M., Hamilton, J. F., Lewis, A. C., Mehra, A., Worrall, S. D.,
925 Bacak, A., Bannan, T. J., Coe, H., Ouyang, B., Jones, R. L., Crilley, L. R., Kramer, L. J.,
926 Bloss, W. J., Vu, T., Kotthaus, S., Grimmond, S., Sun, Y., Xu, W., Yue, S., Ren, L., Acton,
927 W. J. F., Hewitt, C. N., Wang, X., Fu, P., and Heard, D. E.: Evaluating the sensitivity of
928 radical chemistry and ozone formation to ambient VOCs and NO_x in Beijing, *Atmos. Chem.*
929 *Phys. Discuss.*, 21, 2125-2147, <https://doi.org/10.5194/acp-2020-785>, 2021.

930 Wiedensohler, A., Birmili, W., Nowak, A., Sonntag, A., Weinhold, K., Merkel, M., Wehner,
931 B., Tuch, T., Pfeifer, S., Fiebig, M., Fjåraa, A. M., Asmi, E., Sellegri, K., Depuy, R., Venzac,
932 H., Villani, P., Laj, P., Aalto, P., Ogren, J. A., Swietlicki, E., Williams, P., Roldin, P.,
933 Quincey, P., Hüglin, C., Fierz-Schmidhauser, R., Gysel, M., Weingartner, E., Riccobono, F.,
934 Santos, S., Gröning, C., Faloon, K., Beddows, D., Harrison, R., Monahan, C., Jennings, S. G.,
935 O'Dowd, C. D., Marinoni, A., Horn, H. G., Keck, L., Jiang, J., Scheckman, J., McMurry, P.
936 H., Deng, Z., Zhao, C. S., Moerman, M., Henzing, B., de Leeuw, G., Lösschau, G., and
937 Bastian, S.: Mobility particle size spectrometers: harmonization of technical standards and
938 data structure to facilitate high quality long-term observations of atmospheric particle number
939 size distributions, *Atmos. Meas. Tech.*, 5, 657-685, <https://doi.org/10.5194/amt-5-657-2012>,
940 2012.



941 Woodward-Massey, R., Slater, E. J., Alen, J., Ingham, T., Cryer, D. R., Stimpson, L. M., Ye,
942 C., Seakins, P. W., Whalley, L. K., and Heard, D. E.: Implementation of a chemical
943 background method for atmospheric OH measurements by laser-induced fluorescence:
944 characterisation and observations from the UK and China, *Atmos. Meas. Tech.*, 13, 3119-
945 3146, <https://doi.org/10.5194/amt-13-3119-2020>, 2020.

946 Xue, L. K., Wang, T., Gao, J., Ding, A. J., Zhou, X. H., Blake, D. R., Wang, X. F., Saunders,
947 S. M., Fan, S. J., Zuo, H. C., Zhang, Q. Z., and Wang, W. X.: Ground-level ozone in four
948 Chinese cities: precursors, regional transport and heterogeneous processes, *Atmos. Chem.*
949 *Phys.*, 14, 13175-13188, <https://doi.org/10.5194/acp-14-13175-2014>, 2014.

950 Ye, C., Heard, D. E., and Whalley, L. K.: Evaluation of novel routes for NO_x formation in
951 remote regions. , *Environ. Sci. Technol.*, 51, 7442-7449, <https://doi.org/acs.est.6b06441>,
952 2017.

953 Zhou, J., Murano, K., Kohno, N., Sakamoto, Y., and Kajii, Y.: Real-time quantification of the
954 total HO₂ reactivity of ambient air and HO₂ uptake kinetics onto ambient aerosols in Kyoto
955 (Japan), *Atmos. Environ.*, 223, 117189, <https://doi.org/10.1016/j.atmosenv.2019.117189>,
956 2020.

957 Zhou, J., Sato, K., Bai, Y., Fukusaki, Y., Kousa, Y., Ramasamy, S., Takami, A., Yoshino, A.,
958 Nakayama, T., Sadanaga, Y., Nakashima, Y., Li, J., Murano, K., Kohno, N., Sakamoto, Y.,
959 and Kajii, Y.: Kinetics and impacting factors of HO₂ uptake onto submicron atmospheric
960 aerosols during the 2019 Air QUALity Study (AQUAS) in Yokohama, Japan, *Atmos. Chem.*
961 *Phys.*, 21, 12243-12260, <https://doi.org/10.5194/acp-21-12243-2021>, 2021.

962